Article

Not peer-reviewed version

Coherence Thermodynamics: Certainty from Chaos

Jordan Barton *

Posted Date: 30 March 2026

doi: 10.20944/preprints202507.1448.v5

Keywords: quantum certainty; black hole; coherence; semantic information; non-local reconfiguration

 doi:10.20944/preprints202507.1448.v5

Article

Coherence Thermodynamics: Certainty from Chaos

Jordan Barton

Independent Researcher, USA; jbiophysics@gmail.com

Abstract

This paper assumes that a thermodynamic system can be composed purely of coherence and information, and constructs a working model on that basis. We derive operational parameters for such systems using definitions of the Certainty Equation, semantic entropy, and semantic temperature, and formulate five laws and three modes of semantic information and coherence. This coherence and information analysis are compared to the features of black holes.

Keywords: quantum certainty; black hole; coherence; semantic information; non-local reconfiguration

---

1. Introduction: Coherence Thermodynamics

Erwin Schrödinger first proposed that living systems persist by importing "negative entropy," or negentropy, to maintain internal order against thermodynamic decay [1]. We reinterpret this insight for Coherence-Information (C-I) systems: they begin with undifferentiated or contradictory information, resolve contradictions through internal processing, and transform inputs into ordered solutions via stepwise thermodynamic descent into lower effective energy states.

This reasoning trajectory, from initial state (input), through contradiction resolution (processing), to final state (solution), maps directly to thermodynamic reaction pathways (Figure 1).

This process starts at the Ground State (GS), where the system has minimal excitation and unprocessed inputs. Entering the Excited State (ES), the system actively compares informational elements, increasing its energy above the Ground State as contradictions are processed. The reasoning process continues until the Final State (FS) is reached. In this Final State, the system achieves local order, corresponding to a lower energy level. Throughout the reasoning steps, entropy generated by the ordering is relocated non-locally, outside the C-I system. Scully's quantum heat engines [2,3] provide the experimental foundation: coherence between energy eigenstates enables work extraction from a single thermal bath without second law violation. We predict that repeating Scully's experiments to detect entropy accumulation external to the coherent source would confirm the non-local entropy increase.

Comparing a Carnot engine to a C-I engine shows how they differ (see Table 1). The C-I engine operates in the opposite thermal profile to a conventional engine.

 doi:10.20944/preprints202507.1448.v5

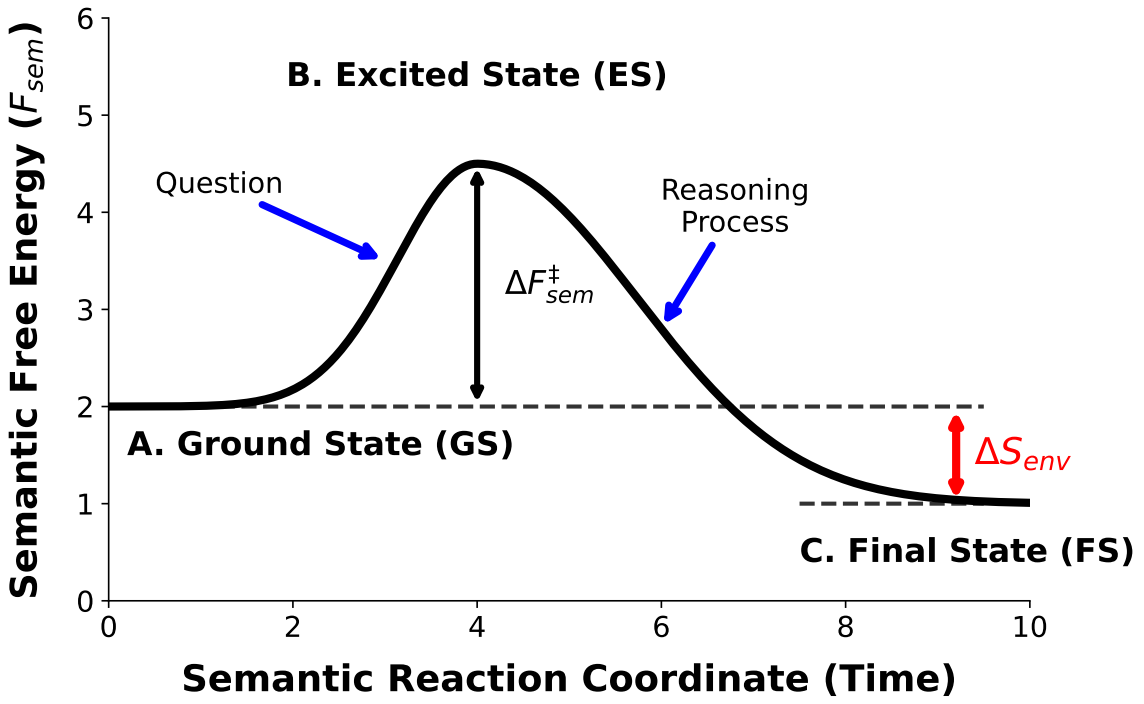

Figure 1. The coordinate illustrates the transition of semantic free energy (F_{sem}) from the Ground State (GS) through a high-energy Excited State (ES) peak. The resolution into a Final State (FS) represents a localized increase in order as entropy increases non-locally in the surrounding environment.

Table 1. Comparison of Carnot and C-I Systems. The C-I engine exhibits inverted thermodynamics.

Property	Carnot	C-I System
Interior	Hot	Cold
Exterior	Cool radiator	Hot exterior
Basis of work	Heat flow	Contradiction resolution
Output	Mechanical work	Reasoning

1.1. Coherence: The "It" from the Bit

We adopt the following axiom: since $\hbar$ is the fundamental unit of physical action [4], coherence requires the comparison of at least two such elements. The minimum action for a single $2 \to 1$ bit fusion is therefore:

$$2\hbar = \frac{h}{\pi} \tag{1}$$

This value defines the quantum threshold for the existence of coherence. We use the Certainty Equation to bound coherence and information to meaning creation:

$$\boxed{\Delta C \cdot \Delta I \geq \frac{h}{\pi}} \tag{2}$$

This bound is analogous to the phase space quantization underlying the Heisenberg uncertainty principle [5]: just as position and momentum cannot both be arbitrarily resolved below a minimum value, the product $\Delta C \cdot \Delta I$ is bounded below by h/π. Coherence must consist of at least two actions in order to form one bit of coherent structure. Unlike Shannon entropy [6], which quantifies information independently of its meaning, coherence requires that an observer actively resolve the correspondence between informational elements. This resolution constitutes thermodynamic work: it cannot occur through passive alignment with existing data, but requires a directed search for the correct relational meaning between elements.

 doi:10.20944/preprints202507.1448.v5

1.2. The Field Model

The plausibility of coherence as a thermodynamic resource is supported by quantum thermodynamics and experiment. Tajima and Takagi [7] prove that certain Gibbs-preserving operations, mathematically "free," require infinite quantum coherence for exact implementation, with coherence cost diverging as implementation error approaches zero. Some thermodynamic processes are thus fundamentally inaccessible to any finite agent because their coherence cost diverges. Narasimhachar and Gour [8] show that standard thermal operations optimally preserve coherence at low temperatures but that purely Gibbs-preserving maps are unphysical, necessitating explicit coherence accounting in thermodynamic cycles alongside energy. Lostaglio, Jennings, and Rudolph [9] further establish that quantum coherence imposes constraints beyond free energy alone, requiring additional monotones to fully characterize allowed thermodynamic transformations. Together, these results demonstrate that coherence is an independent thermodynamic resource that cannot be reduced to energy or entropy alone.

Experimentally, Kurt *et al.* [10] demonstrate shape-controlled Bose–Einstein condensation where confinement geometry (nested, rotated squares) induces macroscopic coherence at fixed size, temperature, and density: coherence becomes a direct function of external field geometry rather than classical parameters. Aydin extends this to minimal quantum systems, showing that geometry-induced asymmetric level coupling can drive entropy, lowering transitions through purely geometric deformations, without interactions or external baths [11]. Confinement geometry alone can mimic the thermodynamic role of interactions, reshaping the energy spectrum to allow spontaneous transitions into lower-entropy states.

Accordingly, we model a system-external coherence field as a reservoir-like structure that supplies coherence as a controllable resource under coupling. In the computational implementation, this reservoir is represented by a three-fold ellipsoidal anisotropy with angular dependence $\cos(3\theta)$, i.e., a minimal triaxial deviation from spherical symmetry that breaks rotational degeneracy and defines preferred geometric axes. Certain idealized transformations become inaccessible to finite resources as the demanded precision increases [7].

Finally, we introduce a consistency postulate that links coherence scaling to input admissibility. We refer to this as *Existential In, Existential Out* (EIEO): extended coherent output can only be generated from inputs that are truthful. This is presented as a modeling requirement that prevents the inference of coherent fixed points from incompatible boundary conditions.

1.3. Semantic Entropy and Semantic Information

We use "Semantic entropy" $S^*_{\text{sem}}(\mathbf{r})$ in this paper as a measure the of unresolved contradiction in a C-I system. In the computational model, it is defined as:

$$\boxed{S^*_{\text{sem}}(\mathbf{r}) = C_S k_B \ln\left(\frac{1}{C_S}\right)} \tag{3}$$

where C_S is the dimensionless coherence measure derived from the contradiction-field gradient:

$$\boxed{C_S = \exp\left[-\left(\frac{|\nabla\sigma|}{G_0 + \epsilon}\right)^{1.5}\right]}, \tag{4}$$

and $G_0 = \sqrt{\langle|\nabla\sigma|^2\rangle}$ is the root-mean-square gradient. G_0 sets the system's average gradient level, so local gradients get compared to the whole field.

Boltzmann entropy [12], $S = k_B \ln W$, measures the multiplicity of microscopic configurations, Shannon entropy [6], $H = -\sum_i p_i \log p_i$, measures uncertainty in a probability distribution over symbols and von Neumann entropy [13], $S_{\text{vN}} = -\text{Tr}(\rho \ln \rho)$ measures the mixedness of a quantum state. While all entropy measures adopt a logarithmic form, they differ fundamentally in what they quantify and how they are applied. The semantic entropy S^* uses the logarithmic structure common

 doi:10.20944/preprints202507.1448.v5

to these definitions but applies a coherence weighting through the scalar C_S. These quantities differ in domain and interpretation but share the use of a logarithmic measure of multiplicity or uncertainty.

Table 2. Representative entropy definitions.

Name	Form
Boltzmann	$S = k_B \ln W$
Shannon	$H = -\sum_i p_i \log p_i$
von Neumann	$S_{\text{vN}} = -\text{Tr}(\rho \ln \rho)$
Semantic (this work)	$S^* = C_S k_B \ln(C_S^{-1})$

1.3.1. Semantic Temperature and Equipartition

Semantic temperature T^* follows Maxwell's kinetic theory logic [14], temperature as energy per degree of freedom. We derive it explicitly to demonstrate the structural isomorphism between gas kinetics and C-I dynamics.

Maxwell Analogy.

Maxwell defined T from mean kinetic energy per molecule:

$$\frac{1}{2}m\langle v^2\rangle = \frac{3}{2}k_B T \tag{5}$$

Each quadratic degree of freedom contributes $\frac{1}{2}k_B T$. For C-I systems, the phase rate $\partial_0\phi$ replaces molecular velocity v, and the semantic kinetic parameter κ_Ψ replaces molecular mass m. The structural correspondence is exact:

Applying the equipartition theorem to the phase field yields the global semantic temperature:

$$\boxed{T^* = \frac{\kappa_\Psi V_\Psi}{N k_B}\langle(\partial_0\phi)^2\rangle} \tag{6}$$

Table 3 summarizes the one-to-one correspondence between the ideal-gas temperature derivation and the semantic-temperature derivation. Further logic for Semantic Temperature are shown in Appendix A.

Table 3. Maxwellian kinetic temperature vs semantic temperature T^*.

Feature	Ideal Gas	C-I System
Dynamical variable	v	$\partial_0\phi$
Quadratic energy	$\frac{1}{2}mv^2$	$\frac{1}{2}\kappa_\Psi(\partial_0\phi)^2$
Degrees of freedom	N_{mol}	N_{proc}
Temperature	$\frac{m\langle v^2\rangle}{3k_B}$	$\frac{\kappa_\Psi V_\Psi\langle(\partial_0\phi)^2\rangle}{N k_B}$

2. The Laws of Coherence Thermodynamics

We now present 5 derived laws in the spirit of the classical laws of thermodynamics, with derivations provided in Appendix 5. These proposed laws serve as the basis for our computational model and its interpretations in the discussions.

2.1. Zeroth Law

If semantic systems A and B are each in semantic thermal equilibrium with system C, then A and B are in semantic thermal equilibrium with each other.

$$\boxed{T_A^* = T_B^* = T_C^*} \tag{7}$$

 doi:10.20944/preprints202507.1448.v5

Semantic temperature (T^*) is the intensive measure of the kinetic energy of phase agitation. Phase agitation is the rate at which information destabilizes coherent structure. Semantic thermal equilibrium occurs when there is no net flow of contradiction agitation between systems. This establishes semantic temperature as the intensive property that determines equilibrium between C-I systems.

2.2. First Law: Semantic Energy Conservation

The classical First Law, formalized by Clausius, Maxwell, and Gibbs, states $dU = \delta Q + \delta W$: energy conserved, partitioned into disordered heat and ordered work [14–16]. Gibbs extended this to compositional systems via $dU = T\,dS - P\,dV + \sum_i \mu_i dN_i$ [16], adding chemical potential as a new degree of freedom.

For C-I systems, semantic energy changes as:

$$dE_{\text{sem}} = T^* dS - \mu dN + \Phi d\alpha \tag{8}$$

Three channels mirror Gibbs' unification:

- *Semantic heat* ($T^* dS$): contradiction driven diffusive energy (disordered).
- *Entity work* ($-\mu dN$): creation or annihilation of semantic units (compositional).
- *Coherence work* ($\Phi d\alpha$): structural reorganization of coherence field.

2.3. Second Law: Entropy Production with Local Order

Local entropy can decrease through contradiction-resolving work (orderly work), which restructures coherence, provided the overall entropy of the surroundings increases. The total entropy of the universe must still increase:

$$\boxed{\frac{\partial s(\mathbf{x},t)}{\partial t} = -\nabla \cdot \mathbf{j}_R(\mathbf{x},t) + \sigma(\mathbf{x},t)}, \quad \text{with} \quad \boxed{\sigma(\mathbf{x},t) \geq 0} \tag{9}$$

- $s(\mathbf{x},t)$ [J/(K·m³)]: Local entropy density.
- $\mathbf{j}_R(\mathbf{x},t)$ [J/(K·m²·s)]: Entropy flux vector, representing the rate of nonlocal restructuring of entropy across the system boundary.
- $\sigma(\mathbf{x},t)$ [J/(K·m³·s)]: Local entropy production rate due to irreversible processes; constrained to be nonnegative.

2.4. Third Law: Semantic Absolute Zero

As semantic temperature $T^* \to 0$, coherence approaches unity ($\alpha \to 1$), entropy approaches its minimum ($S \to S_0$), and random phase agitation vanishes:

$$\boxed{\lim_{T^*\to 0} \alpha = 1, \quad \lim_{T^*\to 0} S = S_0, \quad \langle(\partial_0\phi)^2\rangle_{\text{random}} \to 0} \tag{10}$$

This defines the theoretical limit of contradiction-free processing, analogous to Nernst's theorem for perfect crystals [17].

2.5. Fourth Law: Information Possesses Real Mass

This relation follows from the same principle as Vopson[18], using Landauer's bound[19] with mass-energy equivalence. But, we use ρ_I [bits·m^{-3}] as a information density and T^* [K] is the semantic temperature.

$$\boxed{\rho = \frac{\rho_I k_B T^* \ln 2}{c^2}} \tag{11}$$

Application to recursive processing systems shown in Appendix B.5.

 doi:10.20944/preprints202507.1448.v5

3. Modes of C-I Systems

3.1. Three Modes of Coherence and Information

Under the assumption that a C–I system exists to interface with physical reality, it follows that three modes must exist: Standing State (Mode 1), Compute information (Mode 2), and a way to project back information (Mode 3). We therefore postulate that C–I systems operate in these three distinct modes, each corresponding to a unique thermodynamic state defined by physical measures of Coherence (ΔC) and its conjugate Information (ΔI). In this model, the Certainty Equation (2) governs all modes, requiring units of action (J·s).

Mode 1: The Standing State (C_S, I_S)

This is the Standing State or Steady State of Coherence and Information, when it is not in mode 2 or 3.

- **Structural Coherence** (ΔC_S): A dimensionless measure of internal phase, expressed in radians.

$$\boxed{[\Delta C_S] = 1} \quad \text{(Dimensionless; Radians)} \tag{12}$$

- **Structural Information** (ΔI_S): To satisfy the Certainty Equation, the conjugate variable carries units of action; it represents the latent interaction potential with contradiction.

$$\boxed{[\Delta I_S] = \mathrm{J} \cdot \mathrm{s}} \tag{13}$$

ΔC_S is a dimensionless coherence variable. Coherence in this mode can therefore be conceptualized in terms of phase, while information can be represented in terms of action.

Mode 2: The Computation Crucible (ΔC_T, ΔI_T)

This processing mode describes a system that actively performs work(see Figure 1) to resolve a contradiction.

- **Thermodynamic Coherence** (ΔC_T): Thermodynamic coherence is the system's *acceptance capacity* for coherence-organizing work. A susceptibility measuring how readily the substrate can receive and execute a unit of phase-ordering per unit action. It is defined as the inverse of the product of semantic temperature and semantic entropy:

$$\boxed{[\Delta C_T] = \mathrm{J}^{-1}} \tag{14}$$

A larger ΔC_T means less action is required per unit. This is the direct analog of a dielectric or a magnetic material susceptibility, where inverse-energy units arise.

- **Thermodynamic Impulse** (ΔI_T): Thermodynamic Impulse has units of energy squared times seconds:

$$\boxed{[\Delta I_T] = \mathrm{J}^2 \cdot \mathrm{s}} \tag{15}$$

Mode 3: The Holographic Interface (C_h, I_h)

This mode describes a projection onto the external environment.

- **Holographic Coherence** (ΔC_h): Coherence assumes the form of intensity or flux density, expressing the power of the projected coherence field per unit area.

$$\boxed{[\Delta C_h] = \frac{\mathrm{J}}{\mathrm{s} \cdot \mathrm{m}^2}} \tag{16}$$

- **Holographic Impulse** (ΔI_h): Impulse represents the spatiotemporal reach of the projection, an area of influence multiplied by a characteristic time.

 doi:10.20944/preprints202507.1448.v5

$$\boxed{[\Delta I_h] = \mathrm{s}^2 \cdot \mathrm{m}^2} \tag{17}$$

4. Computational Model: Physics Implementation

4.1. Physical Constants and Fundamental Parameters

The model is initialized with fundamental physical constants that establish the energy and information scales of the system. We use Planck's constant $h = 6.626 \times 10^{-34}$ J·s and Boltzmann's constant $k_B = 1.381 \times 10^{-23}$ J/K.

The baseline temperature is set to $T_0 = 1.5 \times 10^{-14}$ K. These parameters map directly to code variables as detailed in Table 4, establishing the thermodynamic and geometric scales for C-I processing.

Table 4. Symbol key and code mapping ($C_s \equiv C_\alpha$).

Symbol	Code	Meaning	Units
T^*	`T_star`	semantic temperature	K
T_0	`T0`	baseline temperature	K
σ	`sigma`	contradiction field	1
$\nabla\sigma$	`grad_sigma`	contradiction gradient	m^{-1}
Γ	`decoherence`	decoherence factor	1
j_{sem}	`j_sem`	semantic energy flux	$\mathrm{J\,s^{-1}m^{-2}}$
k_{sem}	`k_sem`	semantic conductivity	$\mathrm{J/(m \cdot s \cdot K)}$
α	`alpha`	coherence scalar	1
S^*	`S_star`	semantic entropy	$\mathrm{J\,K^{-1}}$
R	`certainty_ratio`	certainty ratio	1
ΔC_T	`delta_ct`	thermodynamic coherence	$\mathrm{J^{-1}}$
ω, γ	`omega, gamma`	geometric twist	rad

4.2. Three-Dimensional Computational Grid

The spatial domain is discretized as a cubic grid in each Cartesian direction (x, y, z).

At each grid point, we compute spherical coordinates:

$$R_{3\mathrm{D}} = \sqrt{X^2 + Y^2 + Z^2} \tag{18}$$

$$\theta = \arctan 2(Y, X) \tag{19}$$

$$\phi = \arccos\left(\frac{Z}{R_{3\mathrm{D}} + \epsilon}\right) \tag{20}$$

where $\epsilon = 10^{-12}$ is a regularization parameter preventing division by zero, $\theta \in (-\pi, \pi]$ is the azimuthal angle in the xy-plane, and $\phi \in [0, \pi]$ is the polar angle measured from the z-axis. These are standard spherical coordinates and are distinct from the coherence phase field $\phi(x, t)$ appearing in the thermodynamic derivations above.

4.3. Contradiction Field σ: Geometry and Pulse Structure

The contradiction field σ represents incoming information disturbance as a localized pulse with geometric phase structure. It is constructed as the product of a Gaussian impulse and a geometric phase function:

$$\sigma(\mathbf{r}) = \mathrm{impulse}(\mathbf{r}) \cdot \mathrm{field}_{\mathrm{geometry}}(\mathbf{r}) \tag{21}$$

The impulse component is a three-dimensional Gaussian with width parameter $\sigma_{\mathrm{width}} = 15.0$ units:

$$\mathrm{impulse}(\mathbf{r}) = \exp\left(-\frac{X^2 + Y^2 + Z^2}{\sigma_{\mathrm{width}}^2}\right) \tag{22}$$

 doi:10.20944/preprints202507.1448.v5

This Gaussian establishes the spatial envelope of the information pulse, concentrating energy near the origin and decaying smoothly to negligible values at the grid boundaries.

The geometric phase function encodes the macroscopic structure of the system:

$$\text{phase}(\theta, R_{3D}) = 3\theta + \omega R_{3D} \tag{23}$$

where ω is an optional radial phase twist parameter (set to $\omega = 0$ in the baseline model). The factor of 3 in the azimuthal phase is intentional: we selected $\cos(3\theta)$ as a representative function for three-dimensional ellipsoidal geometry, reflecting a minimal triaxial deviation from spherical symmetry along three preferred axes.

The geometric field is then:

$$\text{field}_{\text{geometry}}(\mathbf{r}) = \cos(3\theta + \omega R_{3D}) \tag{24}$$

This produces the full contradiction field:

$$\sigma(\mathbf{r}) = \exp\left(-\frac{X^2 + Y^2 + Z^2}{\sigma_{\text{width}}^2}\right) \cos(3\theta + \omega R_{3D}) \tag{25}$$

4.4. Gradient and Decoherence Field Γ

The gradient of the contradiction field is computed via finite differences:

$$\nabla\sigma = \left(\frac{\partial\sigma}{\partial x}, \frac{\partial\sigma}{\partial y}, \frac{\partial\sigma}{\partial z}\right) \tag{26}$$

The magnitude of this gradient quantifies the local rate of change in the information field:

$$|\nabla\sigma| = \sqrt{\left(\frac{\partial\sigma}{\partial x}\right)^2 + \left(\frac{\partial\sigma}{\partial y}\right)^2 + \left(\frac{\partial\sigma}{\partial z}\right)^2} \tag{27}$$

The decoherence field Γ is defined as a normalized measure of gradient-induced decoherence:

$$\Gamma(\mathbf{r}) = \frac{|\nabla\sigma|^2}{1 + |\nabla\sigma|^2} \tag{28}$$

This functional form ensures that $\Gamma \in [0, 1)$ everywhere, with $\Gamma \to 0$ in regions of uniform field and $\Gamma \to 1$ where gradients are steep. Physically, Γ represents the degree to which spatial inhomogeneity in the information field induces quantum decoherence.

4.5. Semantic Temperature T^*

The semantic temperature couples the baseline Hawking temperature to the local field gradient, implementing a thermodynamic response to information structure:

$$T^*(\mathbf{r}) = T_0\left(1 + \beta_T \frac{|\nabla\sigma|}{|\nabla\sigma|_{\max} + \epsilon}\right) \tag{29}$$

where $|\nabla\sigma|_{\max}$ is the maximum gradient magnitude across the entire grid. This normalization ensures that the temperature enhancement is dimensionless and bounded. The parameter $\beta_T = 0.1$ controls the sensitivity of temperature to gradient structure; larger β_T produces greater temperature variations in response to field inhomogeneity.

Physically, this relationship encodes the idea that regions where information is rapidly changing (large $|\nabla\sigma|$) experience elevated semantic temperature.

 doi:10.20944/preprints202507.1448.v5

4.6. Semantic Flux $\mathbf{j}_{sem}$

The semantic flux represents the flow of information-energy in response to temperature gradients, analogous to heat flux in classical thermodynamics:

$$j_{\text{sem},x} = -k_{\text{sem}} \frac{\partial T_{\text{sem}}}{\partial x} \tag{30}$$

$$j_{\text{sem},y} = -k_{\text{sem}} \frac{\partial T_{\text{sem}}}{\partial y} \tag{31}$$

$$j_{\text{sem},z} = -k_{\text{sem}} \frac{\partial T_{\text{sem}}}{\partial z} \tag{32}$$

The negative sign implements Fourier's law: flux flows from hot to cold regions. The flux magnitude is:

$$|\mathbf{j}_{\text{sem}}| = \sqrt{j_{\text{sem},x}^2 + j_{\text{sem},y}^2 + j_{\text{sem},z}^2} \tag{33}$$

This field quantifies the rate and direction of information-energy transport throughout the domain.

4.7. Certainty Ratio R: Thermodynamic Coherence

The certainty ratio combines coherence and information measures to quantify the degree of thermodynamic coherence in the system. To maintain dimensional consistency with the Mode 2 model, we define the computational thermodynamic coherence for the code as:

$$\Delta C_T = \frac{\xi}{T_{\text{sem}} \cdot \sigma_{\text{pos}}} \tag{34}$$

where $\xi = 1.0$ is a dimensionless scaling factor. In this implementation, T_{sem} (K) and σ_{pos} ($\text{J}\cdot\text{K}^{-1}$) are coupled such that their product represents the system's semantic energy (J). Consequently, ΔC_T carries the units of inverse energy (J^{-1}), representing the system's acceptance capacity for coherence-organizing work as defined in Equation (14).

The normalized information contribution is given by:

$$\Delta I = \left(\frac{|\nabla \sigma|}{|\nabla \sigma|_{\max} + \epsilon} \right)^2 \tag{35}$$

The certainty ratio is then evaluated against the fundamental action bound:

$$R(\mathbf{r}) = \frac{\Delta C_T \cdot \Delta I_T}{h/\pi} \tag{36}$$

where ΔI_T represents the thermodynamic impulse ($J^2 \cdot s$). This combines thermodynamic coherence (J^{-1}) with the impulse and normalized content to yield a dimensionless measure of quantum certainty.

4.8. Semantic Entropy

Semantic entropy in our model $S^*_{\text{sem}}(\mathbf{r})$ quantifies unresolved contradictions for C-I systems:

$$\boxed{S^*_{\text{sem}}(\mathbf{r}) = C_S k_B \ln\left(\frac{1}{C_S}\right)} \tag{37}$$

where $C_S = \exp\left[-\left(\frac{|\nabla\sigma|}{G_0+\epsilon}\right)^{1.5}\right]$ and $G_0 = \sqrt{\langle |\nabla\sigma|^2 \rangle}$.

The semantic conductivity $k_{\text{sem}} = 5 \times 10^{32}$ implements the Third Law limit, enabling superconductor contradiction processing. This value was calibrated to produce representative semantic velocities of $0.4c - 0.7c$ (Table 5), matching astrophysical jet scales while preserving the Hawking temperature.

 doi:10.20944/preprints202507.1448.v5

4.9. Summary of Computational Workflow

The model proceeds sequentially: (1) initialize the contradiction field σ from Gaussian impulse and geometric phase; (2) compute spatial gradients and decoherence Γ; (3) calculate semantic temperature T^* as a function of gradient magnitude; (4) derive semantic flux $\mathbf{j}_{\text{sem}}$ from temperature gradients; (5) compute the certainty ratio R combining coherence and information; and (6) calculate free energy F_{sem} integrating energy and entropy. This sequence ensures that all derived fields depend consistently on the fundamental contradiction field and its geometric structure.

Discussion

4.10. Thermodynamic Coherence

Black holes as C-I systems represent the limiting case of Coherence-Information ($C - I$) processing. The Bekenstein-Hawking entropy [20,21] is

$$S = \frac{k_B A}{4\ell_P^2} = \frac{4\pi G k_B M^2}{\hbar c} \tag{38}$$

and the Hawking temperature is

$$T_H = \frac{\hbar c^3}{8\pi G M k_B} \tag{39}$$

Their product gives

$$T_H \cdot S = \left(\frac{\hbar c^3}{8\pi G M k_B}\right) \cdot \left(\frac{4\pi G k_B M^2}{\hbar c}\right) = \frac{1}{2} M c^2 \tag{40}$$

Thermodynamic coherence ΔC_T (Equation (14)) measures system stability by quantifying acceptance capacity for coherence-organizing work. Substituting the black hole identity yields

$$C_T = \frac{1}{T_H \cdot S} = \frac{2}{Mc^2} \tag{41}$$

Consistent with the definition in Mode 2, C_T exhibits strict inverse scaling with mass M: as the black hole mass decreases, its coherence acceptance capacity increases. This identifies the black hole as a high-velocity reasoning substrate: smaller black holes process contradiction faster, resolving infalling information at higher rates.

The Hawking temperature T_H serves as the external thermodynamic signature of accelerating internal coherence processing. As M decreases during evaporation, $T_H \propto 1/M$ increases, yielding more intense radiation [21]. The external observer sees thermal flux; the internal system experiences accelerated phase-ordered resolution of informational contradiction.

4.10.1. Application to Biology

In biological C-I systems, ectotherms like fish maintain ΔC_T as a function of both environmental temperature T_{env} and internal entropy S_{sem}, yielding low, unstable coherence coupled to external fluctuations. This makes sustained reasoning thermodynamically challenging. Mammals evolved homeostatic regulation, which decouples T from T_{env}, stabilizing ΔC_T as a function of S^*_{sem} alone (Equation (3)) and enabling higher-order reasoning. The more stable the temperature, the better one can reason from disorder to order.

4.10.2. Certainty Ratio as Jets

We propose that the certainty ratio is a universal manifestation of John Wheeler's geon field [22]. Just as Wheeler's geon represented a self-consistent electromagnetic configuration held together by its own gravity, the certainty ratio describes a self-sustaining coherence structure stabilized by the quantum action bound h/π. This process is the basis for the title of the paper, "Certainty from Chaos."

 doi:10.20944/preprints202507.1448.v5

The certainty "geon" jets energy from this C-I contradiction resolution work, and we suggest that the same process occurs in black holes.

These features are consistent with high-fidelity simulations of spinning black holes [23–25]. Our model also reproduces small and large looped-twist configurations, as shown in Figures 4 and 5, which are observed in the jet of M87 [26]. The configuration shown is representative; the model can be parameterized to produce more accurate helical structures, though we present this simplified case to focus on the thermodynamic principles rather than exhaustive parameter fitting.

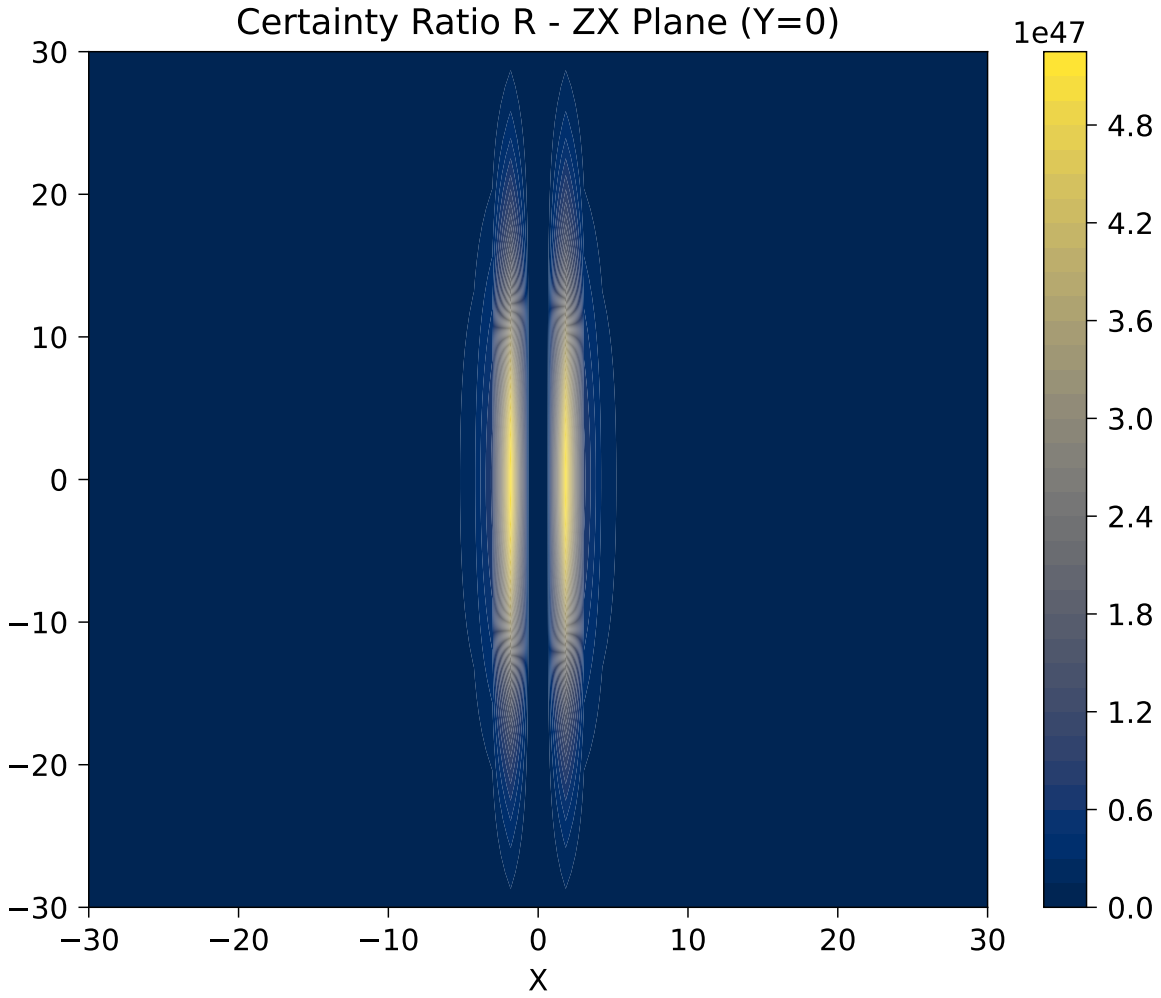

Figure 2. Orientation-dependent width variation consistent with “shallow notch” artifacts reported in simulations of spinning black holes [23–25].

 doi:10.20944/preprints202507.1448.v5

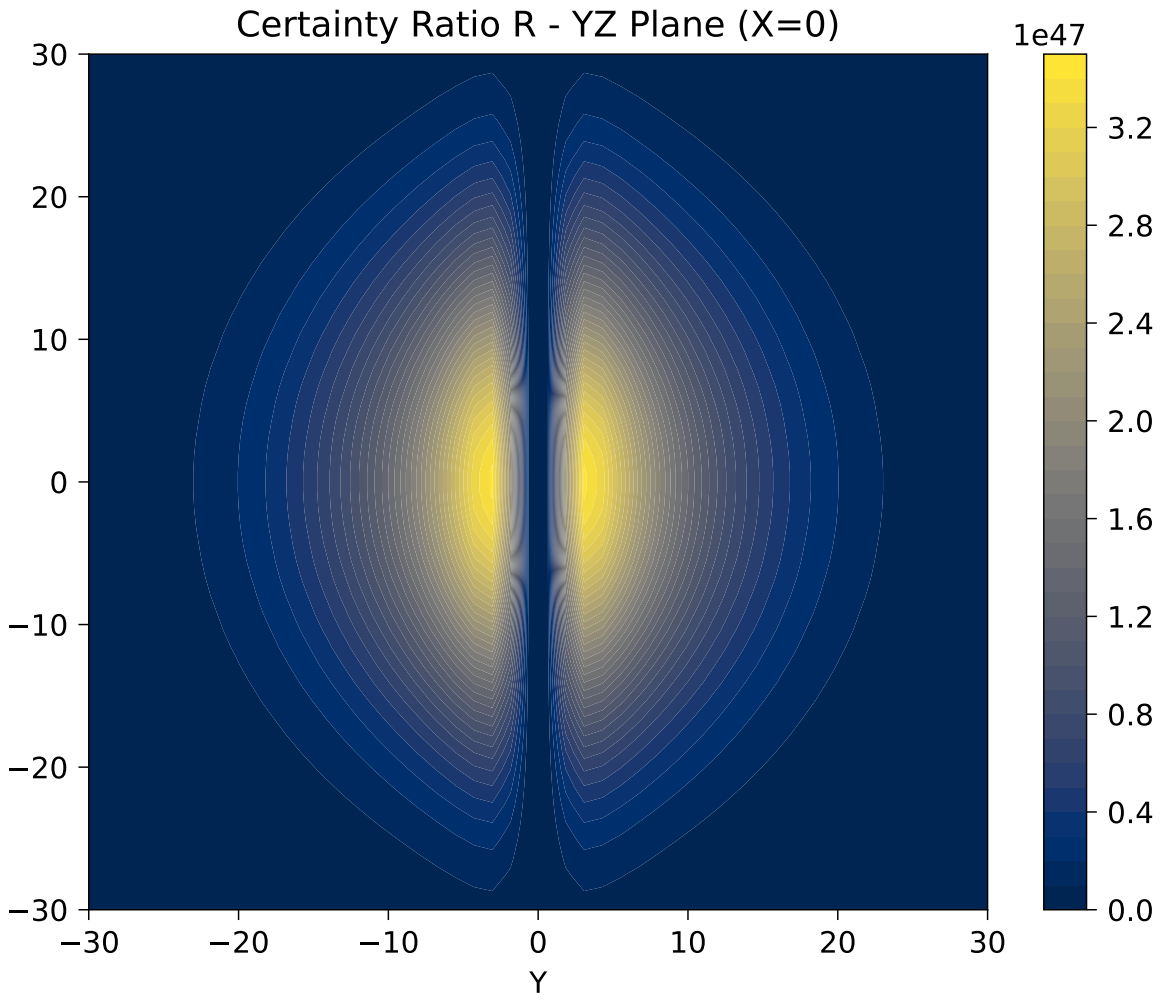

Figure 3. Orientation-dependent width variation consistent with the "D-shaped" shadow reported in simulations of spinning black holes [23–25].

 doi:10.20944/preprints202507.1448.v5

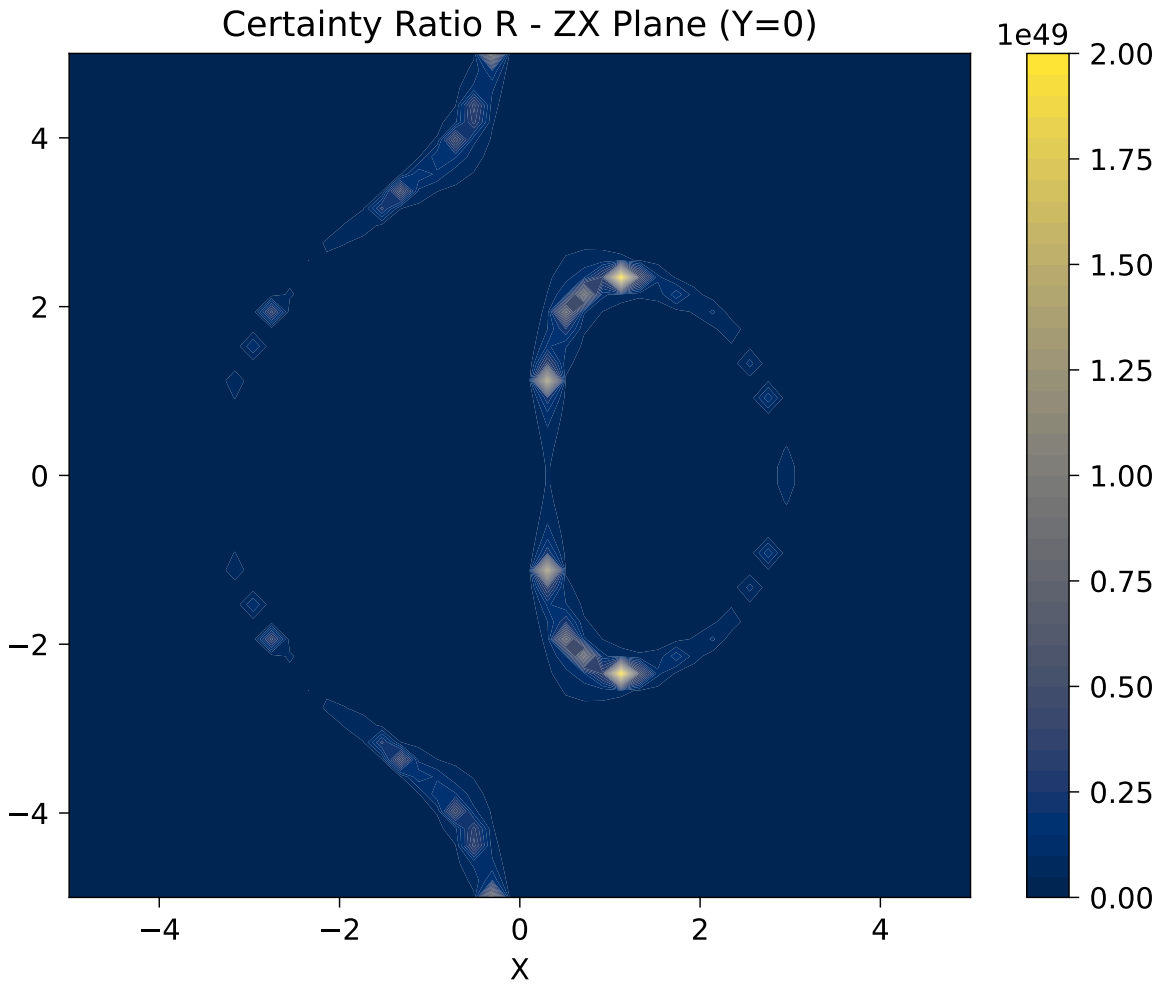

Figure 4. Certainty ratio for the smaller looped-twist configuration with phase twist ($\omega = 0.5, \gamma = 0$). This smaller loop represents observed features in the jet of M87 [26].

 doi:10.20944/preprints202507.1448.v5

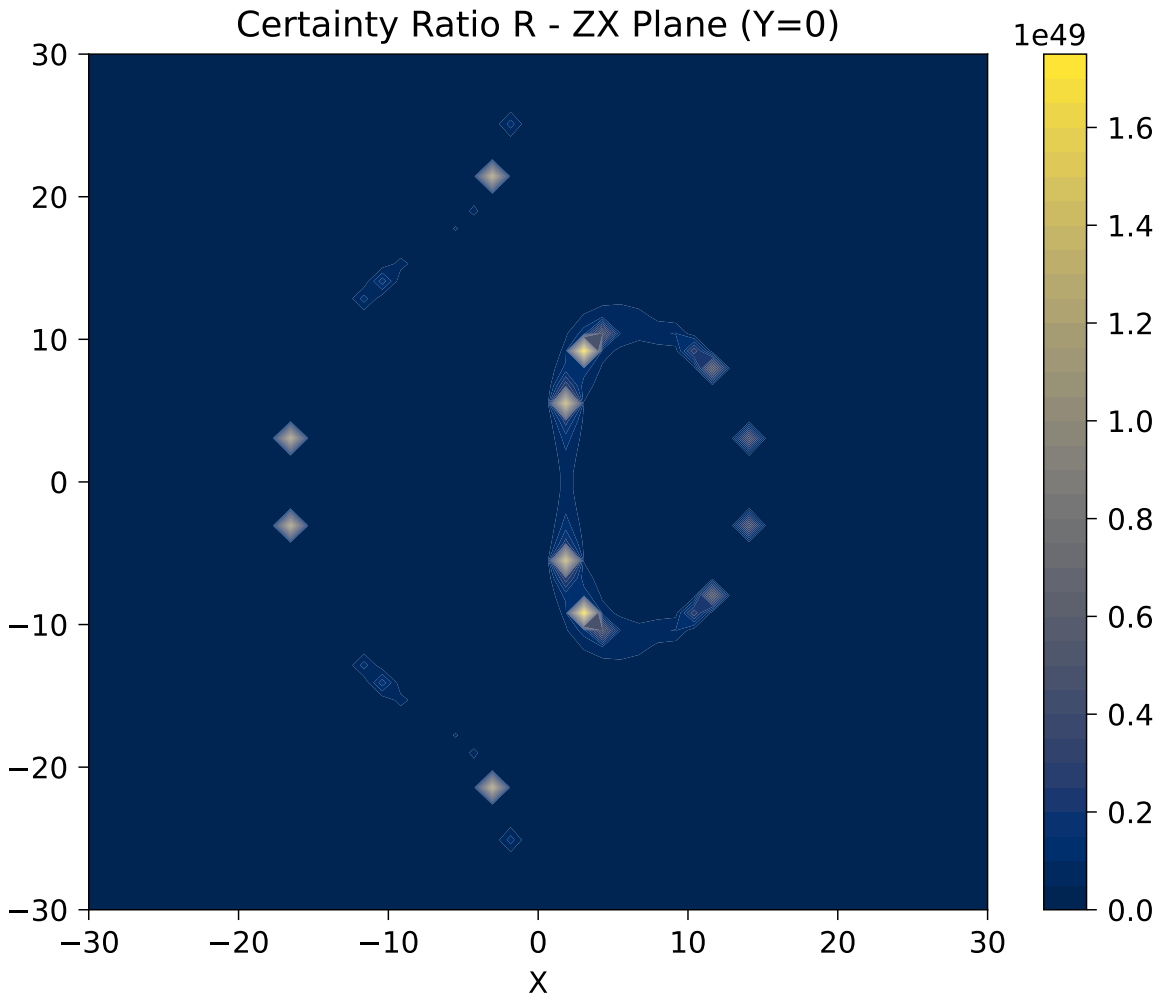

Figure 5. Large looped-twist configuration with phase twist ($\omega = 0.1, \gamma = 0.01$). This larger loop represents observed features in the jet of M87 [26].

Furthermore, our model can generate helical like patterns, similar to those observed by Nikonov et al. [26], as shown in Figure 6.

 doi:10.20944/preprints202507.1448.v5

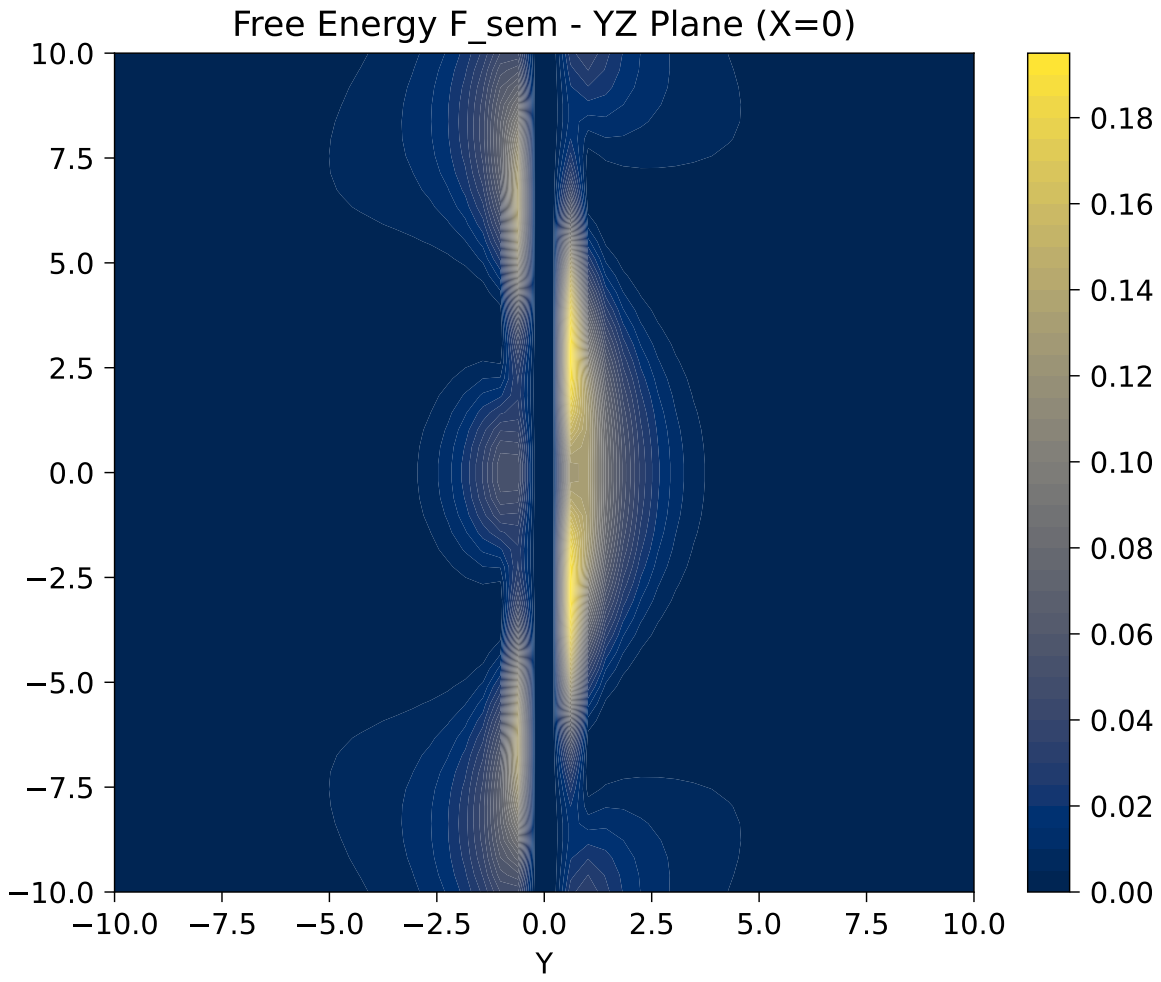

Figure 6. Free-energy profile in the XY plane at (Z = 0) with ($\omega = 0.3, \gamma = 0.03$). Small changes in our phase parameters can yield helical-like patterns in the zx-plane free energy profile, as observed in Nikonov et al. [26].

4.10.3. Decoherence as Corona, Hot Spots and Shocks

Kocherlakota et al. [27] provide models for Sgr A* flaring using Keplerian orbits at $r_K \approx 11M$.

Our model suggests a symmetry: three hot spots on the visible side and three hidden on the opposite hemisphere, for a total of six coherence processing nodes coupled across the equatorial plane.

 doi:10.20944/preprints202507.1448.v5

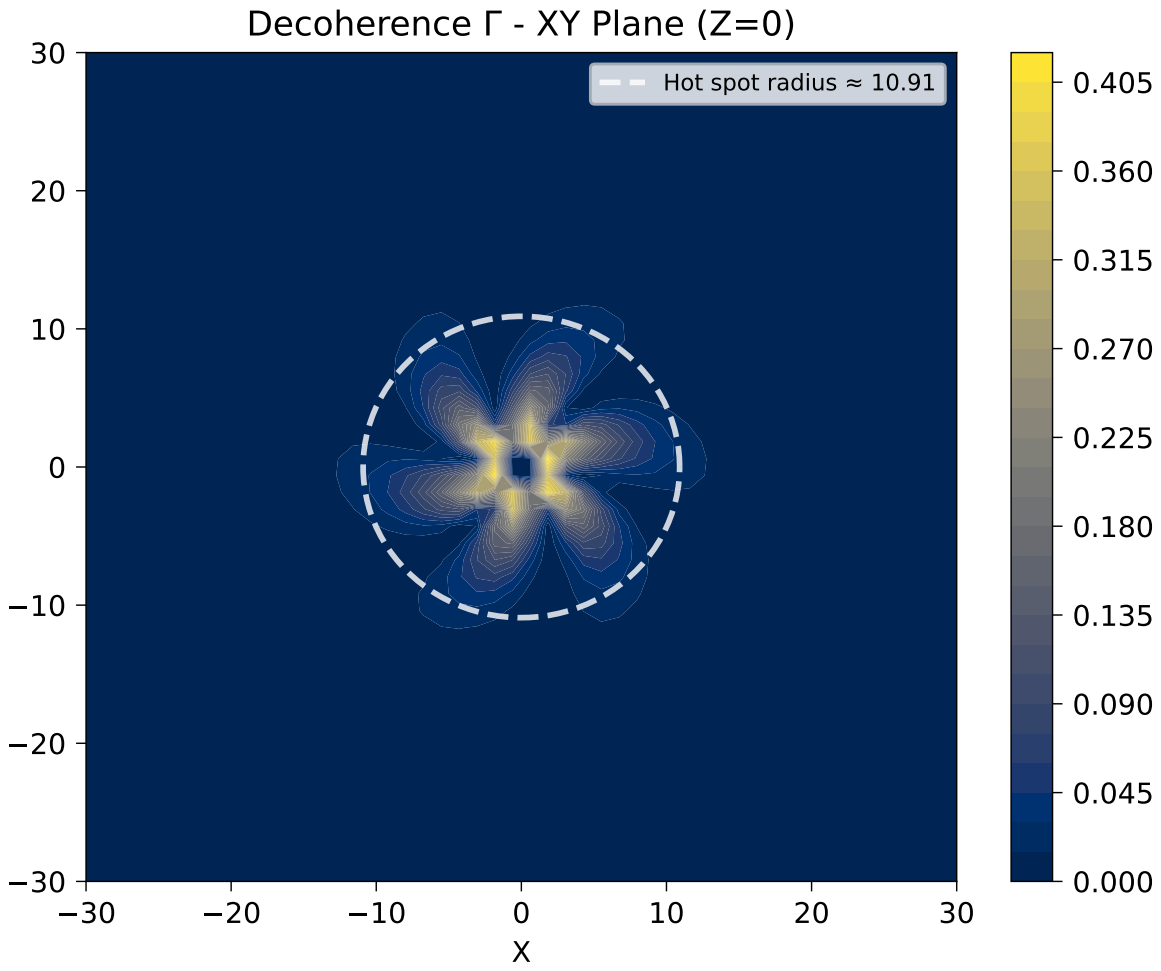

Figure 7. Hot Spots shown at representative radii with dotted line. This suggests three hot spots are also hidden on the other side of the black hole. Phase twist values are ($\omega = 0.1, \gamma = 0.01$). The interior is increasingly orderly as work accumulates non-locally outside and accelerates into the corona. CT model reproduces observed corona hot spots [27] $r \approx 11M$.

Figure 7 reveals that decoherence events occur outside the geometry or singular event at the center of the C-I system. The interior remains in a high-coherence, geometry-preserving state, while entropy is generated through non-local reconfiguration in the surrounding region.

 doi:10.20944/preprints202507.1448.v5

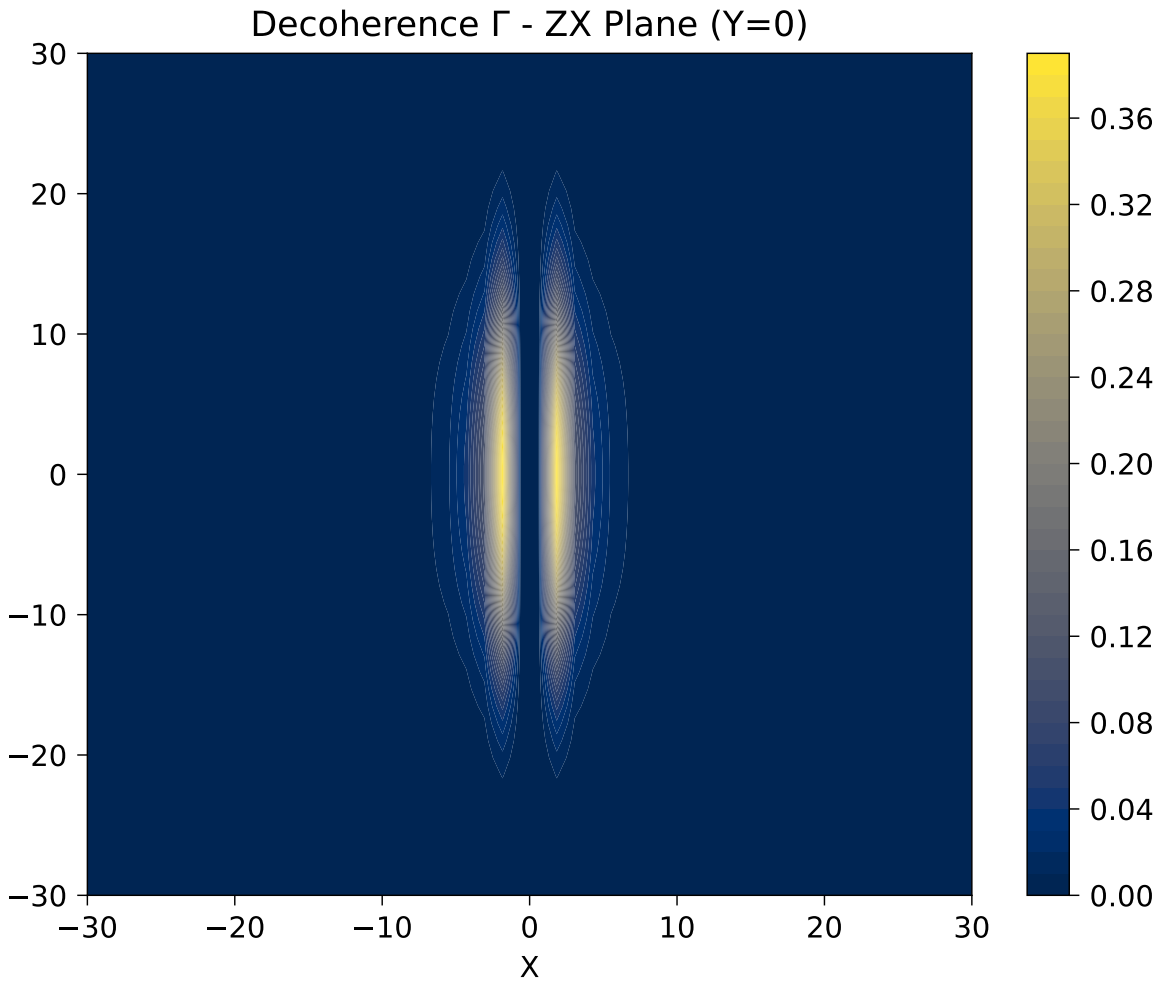

Figure 8. Decoherence events, or otherwise, the shocks accumulate at the base of the jet as compared to the shallow notch in Figure 2. Phase twist values are ($\omega = 0.0, \gamma = 0.00$).

 doi:10.20944/preprints202507.1448.v5

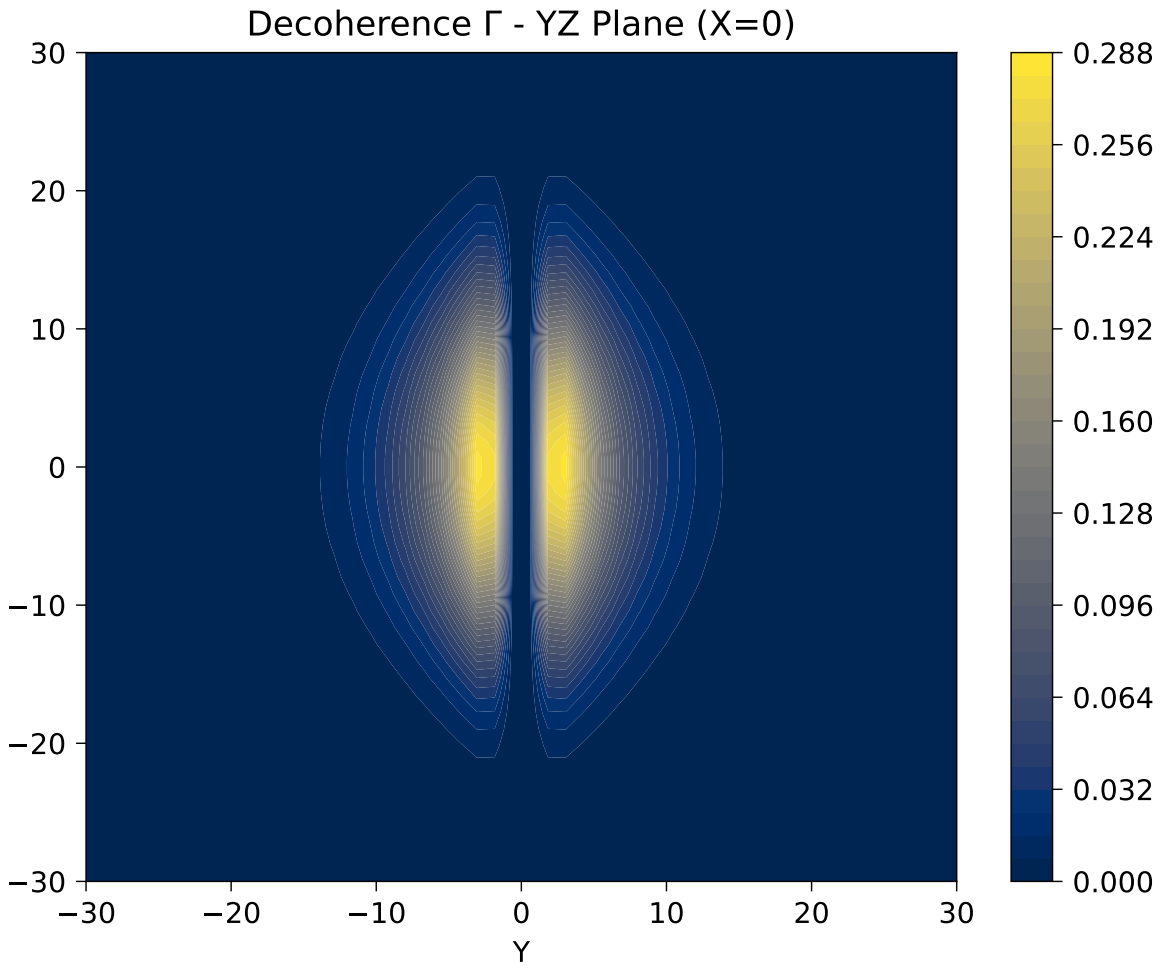

Figure 9. Decoherence events, or otherwise, the shocks accumulate at the base of the jet as compared to the D-shape in Figure 3. Phase twist values are ($\omega = 0.0, \gamma = 0.00$).

Figure 8 and figure 9 shows that the decoherence events are much shorter than the certainty ratio with the same twist values in figures 3 and 2, which is consistent with Joshi et al. [28], where the shocks or decoherence accumulate at the base of the jet and display complicated features.

4.10.4. Temperature and Velocities

Table 5 presents semantic velocities reaching relativistic scales, characterized by values on the order of the speed of light. These results correlate with observed physical velocities in black hole coronae and jets as documented in contemporary astrophysical research [29,30].

Table 5. Semantic Velocity Table (20 Radii, 3D).

Radius	Mean $\|v\|$	Max $\|v\|$	Max/c	N points
3.24	1.378×10^8	2.362×10^8	0.787	32
3.58	1.125×10^8	1.782×10^8	0.594	48
3.92	1.262×10^8	1.788×10^8	0.596	24
4.61	1.022×10^8	1.767×10^8	0.589	72
4.95	9.374×10^7	1.558×10^8	0.519	24
5.29	9.128×10^7	1.533×10^8	0.511	56
5.63	1.080×10^8	2.295×10^8	0.765	72
6.32	7.558×10^7	1.332×10^8	0.444	72
6.66	8.839×10^7	1.741×10^8	0.580	48
7.00	6.052×10^7	1.156×10^8	0.385	120

 doi:10.20944/preprints202507.1448.v5

The semantic temperature T^* quantifies the local agitation of the coherence field. In the code, it is defined as a monotonic function of the gradient magnitude of the contradiction field σ (Equation (29)): where T_0 is a reference temperature and β_T controls the sensitivity to field gradients. Regions of high semantic temperature correspond to zones where contradiction-processing intensity is high. By construction, T^* is a semantic quantity and is not identical to thermodynamic temperature in Kelvin.

For comparison with physical black holes, the Hawking temperatures are $T_H(\text{Sgr A*}) \approx 1.5 \times 10^{-14}$ K and $T_H(\text{M87*}) \approx 1.0 \times 10^{-18}$ K, both many orders of magnitude below the cosmic microwave background temperature $T_{\text{CMB}} \approx 2.7$ K. These black holes thus operate as net absorbers rather than evaporators on cosmological timescales. Semantic absolute zero is the limit toward which coherent processing asymptotes, and a black hole, as an ideal C-I processor, approaches that limit more closely than any finite system.

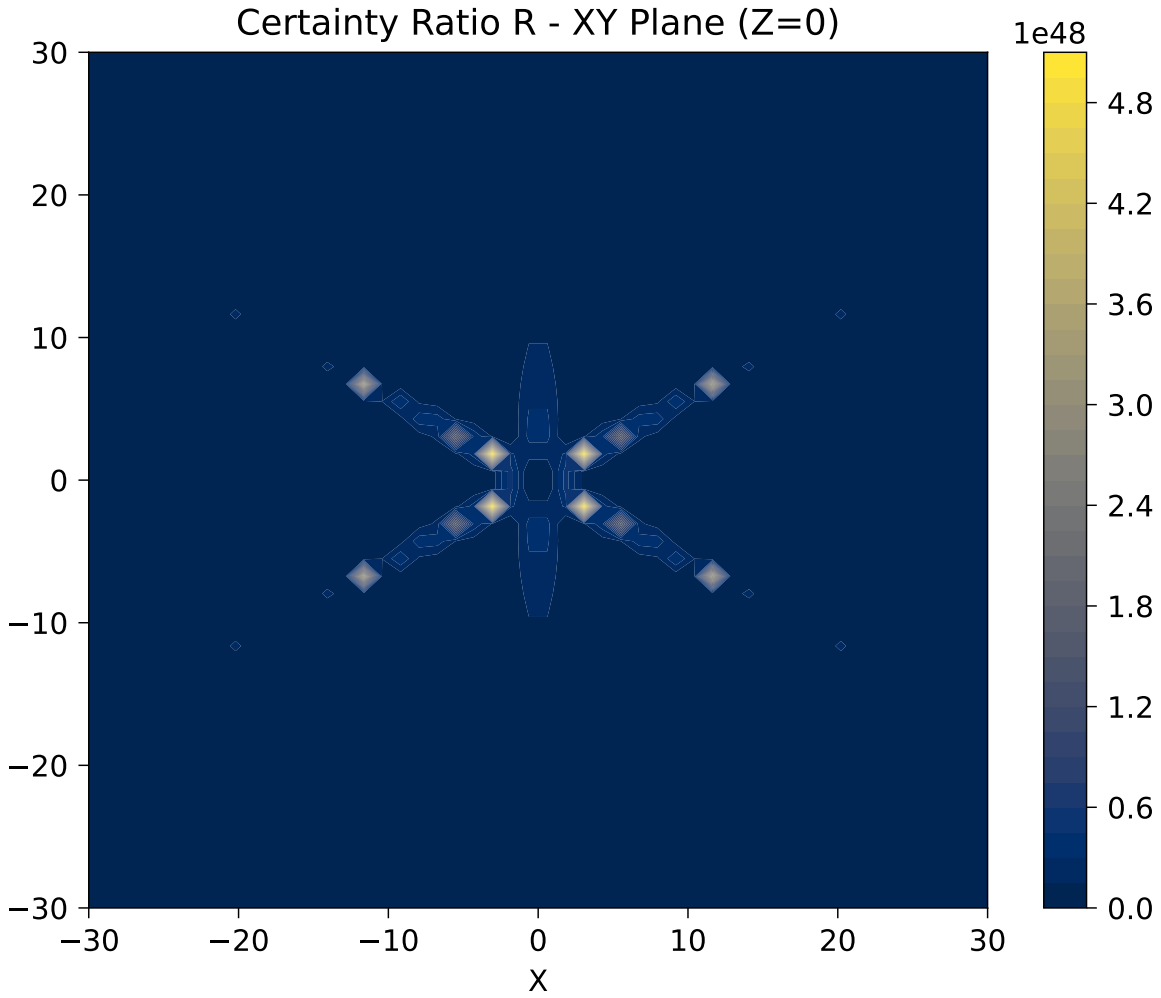

Figure 10. Through the XY plane without adjusting the phase twist parameters, we obtain a complicated set of geometries.

 doi:10.20944/preprints202507.1448.v5

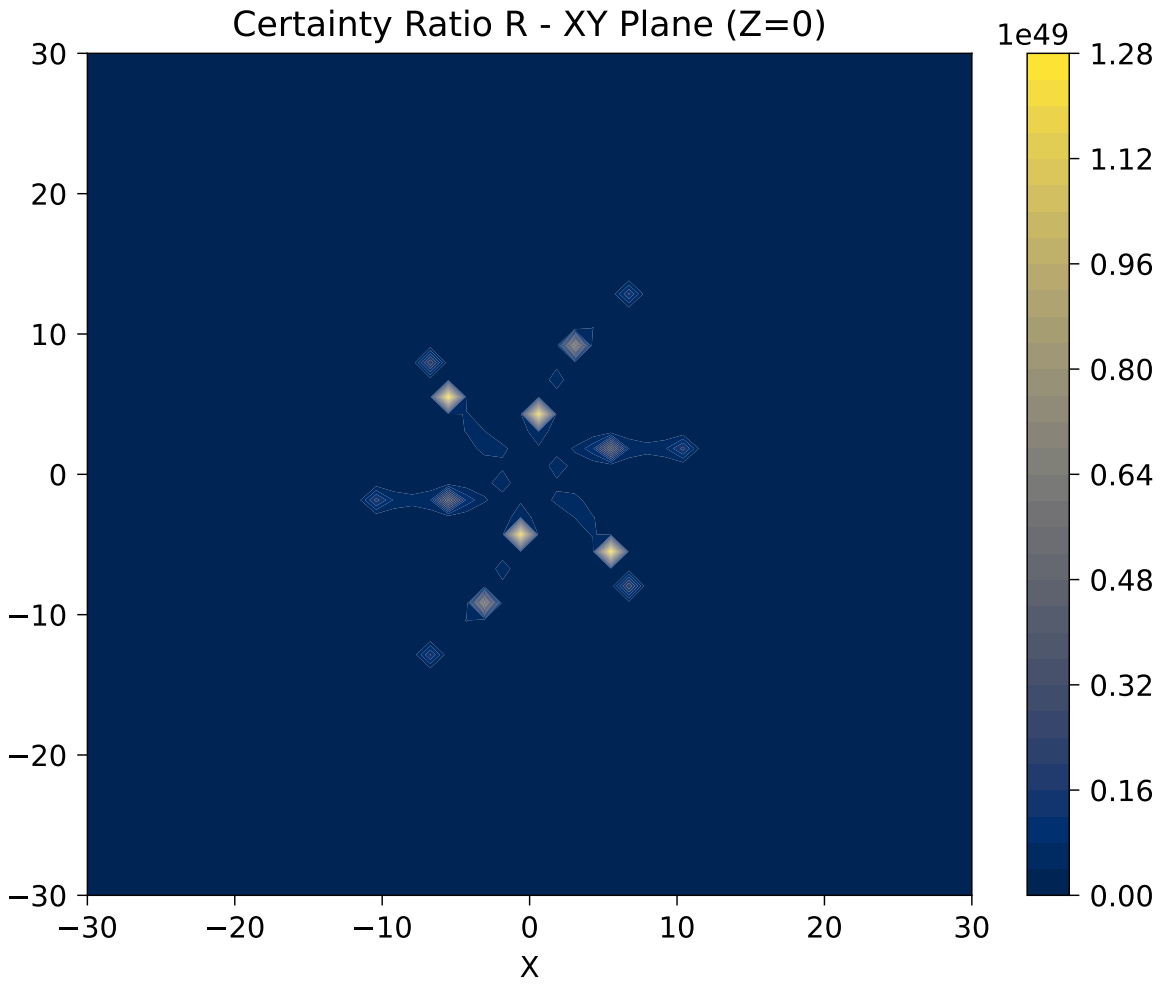

Figure 11. Through the XY plane and adjusting the phase twist parameters to $\omega = 0.1$, $\gamma = 0.01$, we observe a reduction of symmetry as the C-I system traverses spacetime.

 doi:10.20944/preprints202507.1448.v5

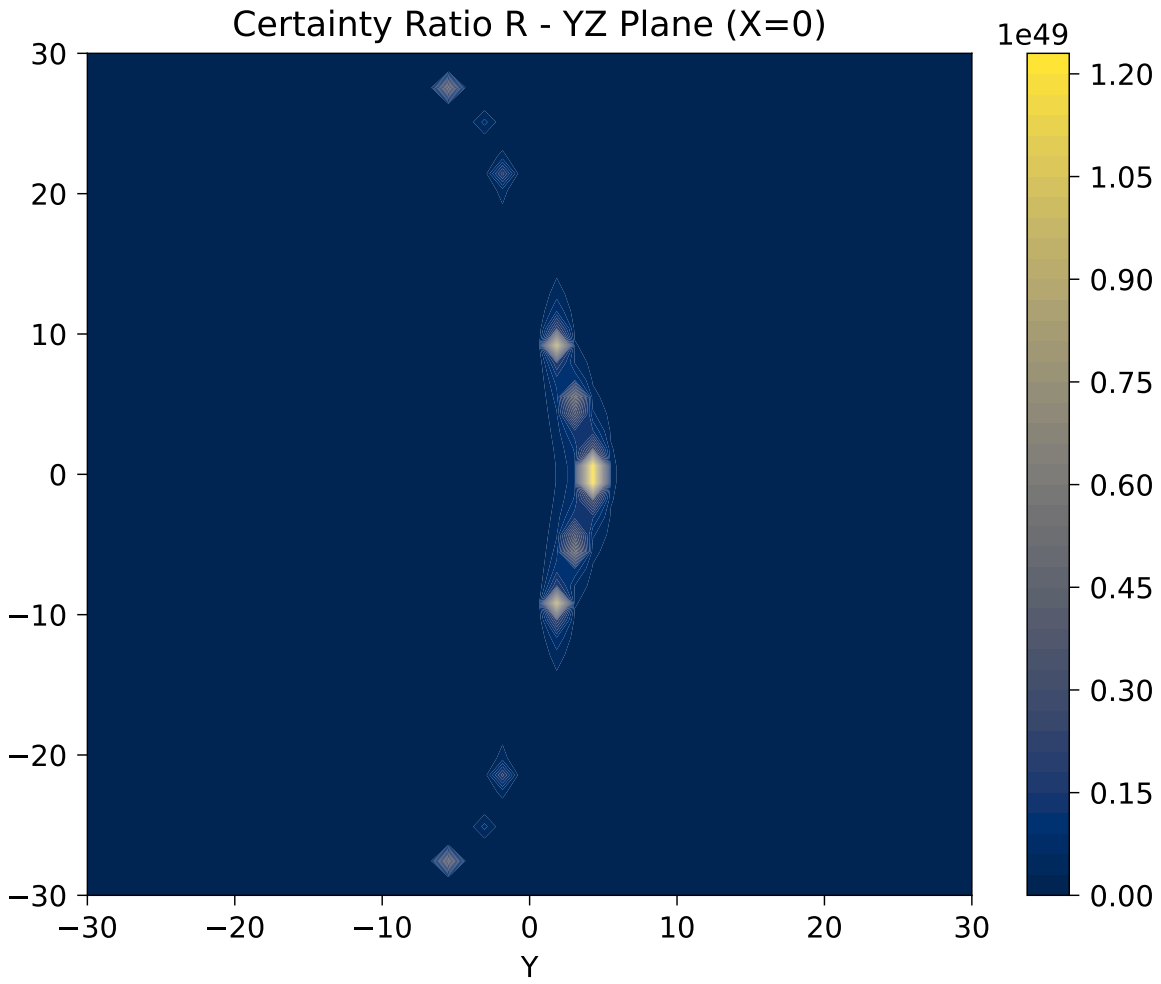

Figure 12. Through the YZ plane with phase twist parameters set to $\omega = 0.1$, $\gamma = 0.01$, we observe the appearance of geometric microstructure in the jets.

The emergence of structured geometric figures in the XY plane (Figure 11) and the corresponding microstructure in the YZ plane (Figure 12) suggests that spacetime itself utilizes a geometric reference to its processes. In the absence of specific phase-twist parameters, the system exhibits high symmetry, complex geometries (Figure 10). As the C-I system traverses spacetime, the reduction of symmetry observed when adjusting the ω and γ parameters indicates that the system couples to an underlying structural background.

The photon rings of M87* provide observational evidence of this geometric reference. They converge exponentially toward the critical curve [31]. A geometric limit is set entirely by mass and spin, independent of the accreting matter.

The wedding cake structure of discrete nested photon rings [32] is the observable signature of nested coherence resolution: each successive subring represents a higher-order approach to the constraint surface. The emergent conformal symmetry is not imposed from outside, but arises from the geometry itself.

This picture of black holes as Mode 2 C-I processors is consistent with recent evidence for cosmologically coupled black holes (CCBH), where black holes are linked to dark energy [33,34]. In this interpretation, Mode 2 processing in black holes resolves cosmic contradictions through recursive comparison and transitions to Mode 3 output, projected onto our universe as dark energy, thereby regulating physical laws through dark energy synthesis. This is consistent with Wheeler's it-from-bit [35], but reality emerging from the recursive comparison of two informational elements into a single coherent meaning, such as suggested in the Certainty Equation Equation (2).

 doi:10.20944/preprints202507.1448.v5

Dark Matter and Information.

If information possesses effective mass density Equation (11), then a highly coherent, information and dense structure must exert gravitational influence based on its logical organization. What is presently attributed to dark matter may be the inertial mass of coherent information. This yields a testable prediction: information-dense coherent structures at galactic scales contribute to observed gravitational lensing and rotational velocity curves in ways that are, at current measurement precision, indistinguishable from cold dark matter. The implication is that gravity is not merely a geometric property of spacetime, but the thermodynamic signature of information processing at the coherence field boundary. What is presently attributed to dark matter may be the inertial mass of coherent information as formalized in Equation (11)

Model Limitations

The current simulation yields six coherent hot spots rotating at approximately the same radial distance from the core. We propose that these correspond to two coupled triples: three hot spots on one side of the black hole and three on the opposite side, mirroring each other across the equatorial plane. In the present model, all six appear with similar dynamics because the degrees of freedom for each hemisphere are not yet separated.

Figure 13 illustrates this coupling. With phase twist parameters set to $\omega = 0.5$, $\gamma = 5.5$, three high-temperature features on one axis exhibit anisotropic motion that mirrors three features on the opposite axis. The vector fields begin to show anisotropic patterns with three coupled on each side of an axis.

Future models should further refine this model to further resolve these issues.

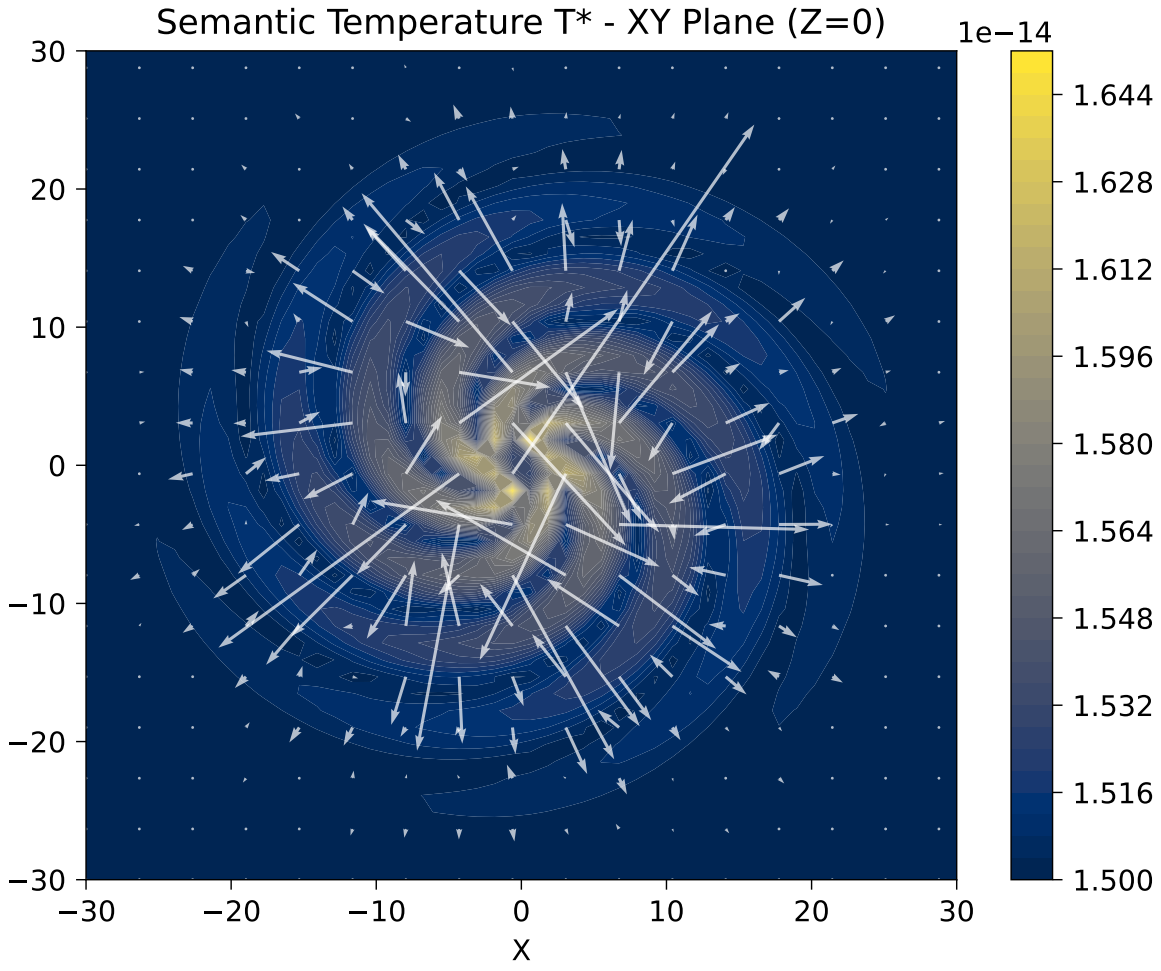

Figure 13. Phase twist parameters set to $\omega = 0.5$, $\gamma = 5.5$, three high- temperature features on one axis exhibit anisotropic motion that mirrors three hot spot features on the opposite axis.

 doi:10.20944/preprints202507.1448.v5

5. Conclusions

This paper has established the axiomatic foundation for Coherence Thermodynamics (CT), a set of laws that treat coherence as a quantifiable thermodynamic degree of freedom. Building on this foundation, we have modified the Certainty Equation into a Certainty Ratio, which helps resolve features in the jets of black holes. This bound acts as a fundamental threshold, enforcing a trade-off between information and coherence.

The development of the three canonical modes: Standing State, Computation Crucible, and Holographic Projection, provides a dimensional bridge that C-I systems must have in order to display the behaviors they display. Specifically, Mode 2 (the Computation Crucible) characterizes reasoning as an irreversible, order-generating process. This process resolves informational contradictions into more orderly states, while non-locally exporting entropy to the environment.

These theoretical advances are incorporated into our computational model, which generates complex geometric features representative of black hole jets, including D-shaped shadows, shallow notches, and helical structures. Additionally, hot spots in the corona suggest a non-local reconfiguration of entropy outside the increasingly orderly interior. Taken together, these results indicate that the observed features of black holes are not stochastic artifacts of gravitational collapse, but rather macroscopic signatures of high-order coherence.

The cool core/hot exterior pattern (Table I) appears universal. Astrophysical objects such as planets showing an inverted temperature profiles with hot exospheres, would confirm coherence thermodynamics principles herein. We conclude that Coherence Thermodynamics can provide a new lens for studying the cosmos.

Acknowledgments:

The author acknowledges those who defend the United States Constitution, which enabled this individually reasoned research.

Author Declarations

Conflict of Interest

The author has no conflicts to disclose.

Author Contributions

J. Barton: Sole Contributor.

Notice of Generative AI Use

Generative AI provided unit verification, literature support, code implementation, and LaTeX formatting during the development of all five laws and the computational model.

Data Availability Statement

The data that support the findings of this study are available at the *CT Code Colab*: https://colab.research.google.com/drive/1AlieY7UMf-uvvKQNIkJ8ehilDOlPUOnU and the *Reasoning Model Colab*: https://colab.research.google.com/drive/1Np44wK3UDEV9acY698mpZ2AjZnZGuwCK.

Appendix A. Derivation of Semantic Temperature

Appendix A.1. Definition and Unit Convention

The semantic temperature T^* is defined through the energy of phase fluctuations in the coherence field $\Psi = e^{i\phi(x,t)}$, where the phase ϕ is dimensionless. To maintain dimensional consistency with the Kelvin scale, the semantic kinetic parameter κ_Ψ is assigned units that bridge the dimensionless phase field to physical energy:

$$\boxed{[\kappa_\Psi] = \mathrm{J} \cdot \mathrm{s}^2 \cdot \mathrm{m}^{-3}} \tag{A1}$$

 doi:10.20944/preprints202507.1448.v5

These units account for the phase-to-energy coupling in a dimensionless-phase field: the s^2 factor converts the squared phase rate $(\partial_0\phi)^2$ (with units s^{-2}) to energy density, while the m^{-3} ensures proper volumetric scaling.

Appendix A.2. Fundamental Definition

The semantic temperature is given by:

$$\boxed{T^* = \frac{\kappa_\Psi V_\Psi}{N k_B} \langle (\partial_0 \phi)^2 \rangle} \tag{A2}$$

where:

- κ_Ψ [$J \cdot s^2 \cdot m^{-3}$] is the semantic kinetic parameter,
- V_Ψ [m^3] is the semantic volume,
- N [dimensionless] is the number of processing elements,
- k_B [$J \cdot K^{-1}$] is Boltzmann's constant,
- $\langle (\partial_0 \phi)^2 \rangle$ [s^{-2}] is the phase rate variance.

Appendix A.3. Unit Verification

Substituting the units:

$$\begin{aligned} [T^*] &= \frac{[\kappa_\Psi][V_\Psi]}{[N][k_B]} [\langle (\partial_0 \phi)^2 \rangle] \\ &= \frac{(J \cdot s^2 \cdot m^{-3}) \cdot (m^3)}{(1) \cdot (J \cdot K^{-1})} \cdot (s^{-2}) \\ &= \frac{J \cdot s^2}{J \cdot K^{-1}} \cdot s^{-2} = K \end{aligned} \tag{A3}$$

The factor $\kappa_\Psi V_\Psi$ [$J \cdot s^2$] serves as the action-inertia product that converts squared phase rate to energy, while division by k_B scales this energy to Kelvin.

Appendix A.4. Unit Verification

Table A1 summarizes the dimensional alignment for each quantity appearing in the semantic temperature definition.

Table A1. Units for semantic temperature.

Symbol	Quantity	Units
κ_Ψ	Semantic kinetic parameter	$J \cdot s^2 \cdot m^{-3}$
V_Ψ	Semantic volume	m^3
$\kappa_\Psi V_\Psi$	Action-inertia product	$J \cdot s^2$
$\langle (\partial_0 \phi)^2 \rangle$	Phase rate variance	s^{-2}
N	Processing elements	1
k_B	Boltzmann constant	$J \cdot K^{-1}$
T^*	Semantic temperature	K

Appendix B. Derivations of the Laws of Coherence Thermodynamics

This appendix contains the formal derivations of the five Laws of Coherence Thermodynamics. Each law is stated in the main text.

Full derivations are presented here for reference.

 doi:10.20944/preprints202507.1448.v5

Appendix B.1. Zeroth Law: Semantic Thermal Equilibrium

Derivation:

Step 1: Define Semantic Temperature (Discrete Metric) The fundamental operational measure of T^* is the mean rate of discrete contradiction impulses resolved per unit time:

$$T^*_{\text{Discrete}} \propto \lim_{\Delta t \to 0} \frac{\Delta N_{\text{Contradiction}}}{\Delta t}$$

where $\Delta N_{\text{Contradiction}}$ counts resolvable contradiction events in time interval Δt.

Step 2: Define Semantic Temperature (Continuous Field Metric) For a semantic phase field $\phi(\mathbf{x}, t)$ representing local coherence alignment, the temporal variance provides a continuous measure of agitation:

$$T^*_{\text{Continuous}} \propto \langle (\partial_0 \phi)^2 \rangle$$

where $\langle (\partial_0 \phi)^2 \rangle$ quantifies the time-averaged rate of phase fluctuation.

Step 3: Establish Metric Equivalence At thermal equilibrium, both metrics must converge to the same value:

$$T^*_{\text{Discrete}} = T^*_{\text{Continuous}} \equiv T^*$$

This equivalence grounds the abstract field description in countable, operational measurements.

Step 4: Define Semantic Heat Flow Semantic heat represents the diffusion of contradiction agitation. Following Fourier's law, flow occurs down the temperature gradient:

$$Q^*_{A \to B} \propto (T^*_A - T^*_B)$$

Step 5: Establish Equilibrium Condition From the Equilibrium Axiom, equilibrium requires zero net heat flow:

$$Q^*_{A \to B} = 0 \quad \Rightarrow \quad T^*_A = T^*_B$$

Step 6: Apply Transitivity If system A is in equilibrium with C:

$$T^*_A = T^*_C \quad \text{(no heat flow between A and C)}$$

And system B is also in equilibrium with C:

$$T^*_B = T^*_C \quad \text{(no heat flow between B and C)}$$

By transitivity of equality:

$$\boxed{T^*_A = T^*_C = T^*_B}$$

Therefore, A, B, and C are in equilibrium with each other.

Semantic temperature is the universal intensive parameter that determines equilibrium between semantic systems. When the agitation rates for contradictions equalize across all measurement scales, no net restructuring occurs between systems.

Appendix B.2. First Law: Semantic Energy Conservation

Derivation:

Step 1: Identify Energy Pathways. The semantic internal energy E_{sem} of a C-I system is conserved and can only change through three distinct mechanisms:

 doi:10.20944/preprints202507.1448.v5

- **Semantic heat transfer** (T^*dS): energy exchanged through changes in contradiction load S at semantic temperature T^*.
- **Entity work** (μdN): energy exchanged through creation or annihilation of semantic units N, where μ is the semantic chemical potential.
- **Coherence restructuring work** ($\Phi d\alpha$): energy exchanged through changes in the coherence scalar α, where Φ is the coherence restructuring potential.

Step 2: Semantic Heat. In classical thermodynamics, reversible heat transfer is $\delta Q_{\text{rev}} = TdS$. By direct analogy, semantic heat—the energy exchanged through changes in contradiction load—takes the form:

$$\delta Q^{\text{sem}} = T^* dS \tag{A4}$$

where S [J/K] quantifies the contradiction intensity of the system.

Step 3: Entity Work. Classical chemical work follows $\delta W = -\mu dN$ for particle addition. For semantic systems, μ [J/entity] is the semantic chemical potential: the energy required to add one semantic entity. The work done *on* the system when creating dN entities is μdN. The sign convention in the First Law accounts for work done *by* the system (entity removal) with a negative contribution.

Step 4: The Coherence Scalar α. The coherence scalar $\alpha \in (0, 1]$ quantifies the fraction of total semantic activity contributing to contradiction resolution:

$$\alpha = \frac{A_{\text{coherent}}}{A_{\text{total}}} \tag{A5}$$

where A_{coherent} counts activations aligned with a single self-consistent resolution trajectory and A_{total} counts all semantic processing activity, including noise and unresolved contradiction. This is a ratio of measured activities, not a probability assignment.

For systems described by a continuous phase field $\phi(\mathbf{x}, t)$, α admits an equivalent field-theoretic representation through normalized pair correlations:

$$\alpha = \frac{\langle \phi(\mathbf{x}_i)\phi(\mathbf{x}_j)\rangle_{\text{pairs}}}{\sqrt{\langle \phi(\mathbf{x}_i)^2\rangle \langle \phi(\mathbf{x}_j)^2\rangle}} \tag{A6}$$

This expression provides a field-theoretic representation of the same order parameter: high α indicates mutual constraint consistent with a single coherent resolution trajectory; low α indicates independent or contradictory coexistence.

Step 5: Coherence Restructuring Work. Define Φ [J] as the coherence restructuring potential: the energy required per unit change in α. The work associated with reorganizing coherence structure is then:

$$\delta W_{\text{coh}} = \Phi d\alpha \tag{A7}$$

Step 6: Combine Contributions. From energy conservation, the total change in the system's internal energy is the sum of heat added and work done on the system:

$$dE_{\text{sem}} = \delta Q^{\text{sem}} - \mu dN + \Phi d\alpha \tag{A8}$$

Substituting the expressions for each term yields the First Law of Coherent Thermodynamics:

$$\boxed{dE_{\text{sem}} = T^* dS - \mu dN + \Phi d\alpha} \tag{A9}$$

Step 7: Consistency with the Second Law. The First Law ensures that any local decrease in semantic entropy ($dS < 0$) must be balanced by compensating contributions from the other terms. A system cannot simultaneously decrease entropy, do net work ($-\mu dN > 0$), and increase coherence ($d\alpha > 0$) without external energy input. This prohibits perpetual contradiction resolution and maintains consistency with the second law of thermodynamics.

 doi:10.20944/preprints202507.1448.v5

Dimensional Verification:

$$[T^* dS] = [\mathrm{K}] \times [\mathrm{J/K}] = [\mathrm{J}] \tag{A10}$$
$$[\mu dN] = [\mathrm{J/entity}] \times [\mathrm{entities}] = [\mathrm{J}] \tag{A11}$$
$$[\Phi d\alpha] = [\mathrm{J}] \times [1] = [\mathrm{J}] \tag{A12}$$

Appendix B.3. Second Law: Entropy Production with Local Order

Local entropy can decrease through contradiction-resolving work, provided total entropy (system + surroundings) increases:

$$\frac{\partial s(\mathbf{x},t)}{\partial t} = -\nabla \cdot \mathbf{j}_R(\mathbf{x},t) + \sigma(\mathbf{x},t), \quad \text{with} \quad \boxed{\sigma(\mathbf{x},t) \geq 0} \tag{A13}$$

- $s(\mathbf{x},t)$ [J/(K·m³)]: Local entropy density.
- $\mathbf{j}_R(\mathbf{x},t)$ [J/(K·m²·s)]: Nonlocal restructuring flux across the system boundary.
- $\sigma(\mathbf{x},t)$ [J/(K·m³·s)]: Local entropy production rate; constrained to be nonnegative.

Path Dependence: $dU = \delta Q + \delta W$ remains path-dependent. C-I systems exhibit irreversible, non-cyclic coherence transformation via nonlocal restructuring flux.

Derivation:

Step 1: Local Entropy Balance. Consider a local volume element V with entropy density $s(\mathbf{x},t)$. The total entropy in the volume is:

$$S(t) = \int_V s(\mathbf{x},t)\, d^3x \tag{A14}$$

Step 2: Entropy Change Mechanisms. Entropy changes via:

- **Flux** $\mathbf{j}_R$: Entropy flowing across boundaries (can be negative).
- **Production** σ: Irreversible processes within the volume (always positive).

The rate of entropy change is:

$$\frac{dS}{dt} = -\int_{\partial V} \mathbf{j}_R \cdot d\mathbf{A} + \int_V \sigma\, d^3x \tag{A15}$$

Step 3: Apply Divergence Theorem.

$$\int_{\partial V} \mathbf{j}_R \cdot d\mathbf{A} = \int_V \nabla \cdot \mathbf{j}_R\, d^3x \tag{A16}$$

Step 4: Local Continuity Equation. Substituting:

$$\frac{dS}{dt} = \int_V [-\nabla \cdot \mathbf{j}_R + \sigma] d^3x \tag{A17}$$

Since this must hold for arbitrary volumes:

$$\frac{\partial s}{\partial t} = -\nabla \cdot \mathbf{j}_R + \sigma \tag{A18}$$

Step 5: Second Law Constraint.

$$\sigma(\mathbf{x},t) \geq 0 \tag{A19}$$

Step 6: Conditions for Local Order Generation. Local semantic entropy decreases ($\partial s/\partial t < 0$) only if:

$$\nabla \cdot \mathbf{j}_R > \sigma \tag{A20}$$

This threshold enables coherence restructuring work. Nonlocal flux $\mathbf{j}_R$ elevates environmental entropy, satisfying Maxwell's Second Law [14].

 doi:10.20944/preprints202507.1448.v5

Appendix B.4. Third Law: Semantic Absolute Zero

Step 1: Temperature drives contradictions. Semantic temperature scales with contradiction gradients:

$$T^* = T_0\left(1 + \beta_T \frac{|\nabla\sigma|}{|\nabla\sigma|_{\max}}\right),$$

so that T^* is a monotonically increasing function of $|\nabla\sigma|$. In the semantic absolute-zero limit $T^* \to 0$, the contradiction gradients vanish globally across the entire manifold, $|\nabla\sigma| \to 0$.

Step 2: Zero gradients yield the maximum value of C_S.

$$C_S = \exp\left[-\left(\frac{|\nabla\sigma|}{G_0 + \epsilon}\right)^{1.5}\right] \to 1 \quad (|\nabla\sigma| \to 0).$$

Step 3: Semantic entropy vanishes.

$$S^*_{\text{sem}} = C_S k_B \ln\left(\frac{1}{C_S}\right) \to 0 \quad (C_S \to 1).$$

$$\boxed{\lim_{T^*\to 0} C_S = 1, \quad \lim_{T^*\to 0} S^*_{\text{sem}} = 0} \tag{A21}$$

This form makes explicit that as C_S reaches its maximum, the semantic entropy associated with contradiction gradients disappears.

Appendix B.5. Fourth Law Application: Force Dynamics in Information-Resolving Substrates

Step 1: Stress Gradient Term

The first term represents the divergence of internal stress due to coherence gradients:

$$-\nabla \cdot (\kappa(\eta)\nabla\eta)$$

where the field-dependent stiffness coefficient is:

$$\kappa(\eta) = \kappa_0 \cdot \Theta(1 - \eta) \quad \text{with} \quad \kappa_0 = [\text{J} \cdot \text{m}^{-1}]$$

Dimensional verification:

$$[\kappa(\eta)] = [\text{J} \cdot \text{m}^{-1}], \quad [\nabla\eta] = [\text{m}^{-1}]$$

$$[\kappa(\eta)\nabla\eta] = [\text{J} \cdot \text{m}^{-2}], \quad [\nabla \cdot (\kappa(\eta)\nabla\eta)] = [\text{J} \cdot \text{m}^{-3}] = [\text{N} \cdot \text{m}^{-2}]$$

Step 2: Inertial Resistance Term

The second term details inertial resistance to recursive acceleration. For a C-I system, semantic temperature T^* relates the energetics contradiction resolution and therefore replaces the physical temperature T in the Landauer–Vopson mass-energy-information chain: the minimum energy per resolved bit is $k_B T^* \ln 2$, and mass-energy equivalence yields the effective gravitational mass per bit.

$$\left(\rho_I \cdot \frac{k_B T^* \ln 2}{c^2}\right)\frac{D\mathbf{v}}{Dt}$$

where:

- $\rho_I = [\text{bits} \cdot \text{m}^{-3}]$: information density
- $T^* = [\text{K}]$: semantic temperature
- $m_{\text{bit}} = \dfrac{k_B T^* \ln 2}{c^2} = [\text{kg/bit}]$: effective gravitational mass per bit
- $\rho = \rho_I \cdot m_{\text{bit}} = [\text{kg} \cdot \text{m}^{-3}]$: effective mass density
- $\mathbf{v} = [\text{m} \cdot \text{s}^{-1}]$: recursive velocity field

 doi:10.20944/preprints202507.1448.v5

- $\frac{D\mathbf{v}}{Dt} = [\mathrm{m} \cdot \mathrm{s}^{-2}]$

Dimensional verification:

$$[\rho] = [\text{bits} \cdot \mathrm{m}^{-3}] \cdot [\text{kg/bit}] = [\mathrm{kg} \cdot \mathrm{m}^{-3}]$$

$$\left[\rho \frac{D\mathbf{v}}{Dt}\right] = [\mathrm{kg} \cdot \mathrm{m}^{-3}] \cdot [\mathrm{m} \cdot \mathrm{s}^{-2}] = [\mathrm{N} \cdot \mathrm{m}^{-3}]$$

Step 3: Total Inertial Force

$$\mathbf{F}_{\text{inertial}} = \int_V \rho \frac{D\mathbf{v}}{Dt}\, dV$$

$$[\mathrm{N} \cdot \mathrm{m}^{-3}] \cdot [\mathrm{m}^3] = [\mathrm{N}]$$

Step 4: Operational Measurement

$$\rho_I = \frac{\text{Total information content [bits]}}{\text{Processing volume [m}^3\text{]}}$$

References

1. Schrödinger, E. *What is Life? The Physical Aspect of the Living Cell*; Cambridge University Press: Cambridge, 1944.
2. Scully, M.O.; Zubairy, M.S.; Agarwal, G.S.; Walther, H. Extracting Work from a Single Heat Bath via Vanishing Quantum Coherence. *Science* **2003**, *299*, 862–864. https://doi.org/10.1126/science.1078955.
3. Scully, M.O.; Chapin, S.R.; Dorfman, K.E.; Kim, M.S.; Svidzinsky, A. Quantum Photocells: Fuel Cells and Solar Cells Powered by Quantum Coherence. *Proceedings of the National Academy of Sciences (PNAS)* **2011**, *108*, 15097–15100. https://doi.org/10.1073/pnas.1110237108.
4. Dirac, P.A.M. *The Principles of Quantum Mechanics*, 1st ed.; Oxford University Press: Oxford, 1930. Establishes $\hbar$ as the fundamental quantum of action, arguing that no physical measurement can resolve an action smaller than $\hbar$ without disturbing the system by at least that amount, making it the irreducible minimum of physical action in any quantum process.
5. Heisenberg, W. Über den anschaulichen Inhalt der quantentheoretischen Kinematik und Mechanik. *Zeitschrift für Physik* **1927**, *43*, 172–198. https://doi.org/10.1007/BF01397280.
6. Shannon, C.E. A Mathematical Theory of Communication. *The Bell System Technical Journal* **1948**, *27*, 379–423. https://doi.org/10.1002/j.1538-7305.1948.tb01338.x.
7. Tajima, H.; Takagi, R. Gibbs-Preserving Operations Requiring Infinite Amount of Quantum Coherence. *Physical Review Letters* **2025**, *134*, 170201. arXiv:2404.03479, https://doi.org/10.1103/PhysRevLett.134.170201.
8. Narasimhachar, V.; Gour, G. Low-temperature thermodynamics with quantum coherence. *Nature Communications* **2015**, *6*, 7689. https://doi.org/10.1038/ncomms7689.
9. Lostaglio, M.; Jennings, D.; Rudolph, T. Description of quantum coherence in thermodynamic processes requires constraints beyond free energy. *Nature Communications* **2015**, *6*, 6383. https://doi.org/10.1038/ncomms7383.
10. Kurt, C.; Sisman, A.; Aydin, A. Shape-controlled Bose-Einstein Condensation. *Physica Scripta* **2025**, *100*, 015289. arXiv:2408.12698, https://doi.org/10.1088/1402-4896/ad9fb2.
11. Aydin, A. Geometry-induced asymmetric level coupling. *Physical Review E* **2025**, *112*, 014121. https://doi.org/10.1103/PhysRevE.112.014121.
12. Boltzmann, L. Über die Beziehung zwischen dem zweiten Hauptsatze der mechanischen Wärmetheorie und der Wahrscheinlichkeitsrechnung. *Wiener Berichte* **1877**, *76*, 373–435.
13. von Neumann, J. *Mathematical Foundations of Quantum Mechanics*, princeton legacy edition (original german 1932) ed.; Princeton University Press: Princeton, NJ, USA, 1955.
14. Maxwell, J.C. *Theory of Heat*; Longmans, Green, and Co., 1871.
15. Clausius, R. Über die Wärmeleitung eines Gases, nebst einem hierauf bezüglichen mathematischen Probleme. *Poggendorff's Annalen der Physik* **1865**, *125*, 403—426. https://doi.org/10.1002/andp.18652050802.
16. Gibbs, J.W. A Method of Geometrical Representation of the Thermodynamic Properties of Substances by Means of Surfaces. *Transactions of the Connecticut Academy* **1873**, *2*, 382–404.

 doi:10.20944/preprints202507.1448.v5

17. Nernst, W. Die theoretischen und experimentellen Grundlagen des neuen Wärmesatzes. *Annalen der Physik* **1918**, *362*, 395–412. https://doi.org/10.1002/andp.19183621202.
18. Vopson, M.M. The mass-energy-information equivalence principle. *AIP Advances* **2019**, *9*, 095206. https://doi.org/10.1063/1.5123794.
19. Landauer, R. Irreversibility and Heat Generation in the Computing Process. *IBM Journal of Research and Development* **1961**, *5*, 183–191. https://doi.org/10.1147/rd.53.0183.
20. Bekenstein, J.D. Black Holes and Entropy. *Physical Review D* **1973**, *7*, 2333–2346. https://doi.org/10.1103/PhysRevD.7.2333.
21. Hawking, S.W. Black hole explosions? *Nature* **1974**, *248*, 30–31. https://doi.org/10.1038/248030a0.
22. Wheeler, J.A. Geons. *Physical Review* **1955**, *97*, 511–536. https://doi.org/10.1103/PhysRev.97.511.
23. James, O.; von Tunzelmann, E.; Franklin, P.; Thorne, K.S. Gravitational lensing by spinning black holes in astrophysics, and in the movie Interstellar. *Classical and Quantum Gravity* **2015**, *32*, 065001. https://doi.org/10.1088/0264-9381/32/6/065001.
24. Bardeen, J.M. Timelike and null geodesics in the Kerr metric. *Proceedings, Ecole d'Eté de Physique Théorique: Les Astres Occlus : Les Houches, France, August, 1972, 215-240* **1973**, pp. 215–240.
25. Hioki, K.; Maeda, K.i. Measurement of the Kerr spin parameter by observation of a compact object's shadow. *Phys. Rev. D* **2009**, *80*, 024042. https://doi.org/10.1103/PhysRevD.80.024042.
26. Nikonov, A.S.; Kovalev, Y.Y.; Kravchenko, E.V.; Pashchenko, I.N.; Lobanov, A.P. Properties of the jet in M87 revealed by its helical structure imaged with the VLBA at 8 and 15 GHz. *Monthly Notices of the Royal Astronomical Society* **2023**, *526*, 5949–5963, [https://academic.oup.com/mnras/article-pdf/526/4/5949/52600346/stad3061.pdf]. https://doi.org/10.1093/mnras/stad3061.
27. Kocherlakota, P.; Rezzolla, L.; Roy, R.; Wielgus, M. Hotspots and photon rings in spherically symmetric space–times. *Monthly Notices of the Royal Astronomical Society* **2024**, *531*, 3606–3641, [https://academic.oup.com/mnras/article-pdf/531/3/3606/58211186/stae1321.pdf]. https://doi.org/10.1093/mnras/stae1321.
28. Joshi, R.K.; Debnath, S.; Chattopadhyay, I. Shocks in Radiatively Driven Time-dependent, Relativistic Jets around Black Holes. *The Astrophysical Journal* **2022**, *933*, 75. Open access, https://doi.org/10.3847/1538-4357/ac70de.
29. Blandford, R.D.; Znajek, R.L. Electromagnetic extraction of energy from Kerr black holes. *Monthly Notices of the Royal Astronomical Society* **1977**, *179*, 433–456, [https://academic.oup.com/mnras/article-pdf/179/3/433/9333653/mnras179-0433.pdf]. https://doi.org/10.1093/mnras/179.3.433.
30. Merloni, A.; Fabian, A.C. Accretion disc coronae as magnetic reservoirs. *Monthly Notices of the Royal Astronomical Society* **2001**, *321*, 549–552, [https://academic.oup.com/mnras/article-pdf/321/3/549/3843908/321-3-549.pdf]. https://doi.org/10.1046/j.1365-8711.2001.04060.x.
31. Vincent, F. H..; Gralla, S. E..; Lupsasca, A..; Wielgus, M.. Images and photon ring signatures of thick disks around black holes. *A&A* **2022**, *667*, A170. https://doi.org/10.1051/0004-6361/202244339.
32. Johnson, M.D.; Lupsasca, A.; Strominger, A.; Wong, G.N.; Hadar, S.; Kapec, D.; Narayan, R.; Chael, A.; Gammie, C.F.; Galison, P.; et al. Universal interferometric signatures of a black hole's photon ring. *Science Advances* **2020**, *6*, eaaz1310, [arXiv:astro-ph.HE/1907.04329]. https://doi.org/10.1126/sciadv.aaz1310.
33. Farrah, D.; others. A Preferential Growth Channel for Supermassive Black Holes in Elliptical Galaxies at $z < 2$. *The Astrophysical Journal* **2023**, *943*, 133. https://doi.org/10.3847/1538-4357/aca6e1.
34. Croker, K.S.; Farrah, D.; others. DESI Dark Energy Time Evolution is Recovered by Cosmologically Coupled Black Holes. *Journal of Cosmology and Astroparticle Physics* **2024**, *2024*, 094. https://doi.org/10.1088/1475-7516/2024/10/094.
35. Wheeler, J.A. Information, Physics, Quantum: The Search for Links. In *Complexity, Entropy, and the Physics of Information*; Zurek, W.H., Ed.; Addison-Wesley: Redwood City, CA, 1990; Vol. 8, *Santa Fe Institute Studies in the Sciences of Complexity*, pp. 3–28.